849d

NX
R-90.8

INTERIM REPORT ON

LUNAR ORBITER
VISUAL OBSERVATION INSTRUMENT SUBSYSTEM

CONTRACT NO. 950005

7 NOVEMBER 1960

under NASw - 6

TO
JET PROPULSION LABORATORY
CALIFORNIA INSTITUTE OF TECHNOLOGY
PASADENA, CALIFORNIA

BY

ASTRO-ELECTRONICS DIVISION
RADIO CORPORATION OF AMERICA
PRINCETON, NEW JERSEY

RCA

TABLE OF CONTENTS

LIST OF ILLUSTRATIONS

LIST OF ILLUSTRATIONS (Cont.)

I. INTRODUCTION

The VOIS package is designed to accomplish several functions. Of these functions, the mapping of the entire surface of the moon at a reasonably high resolution and the observation of selected areas of the lunar surface at higher resolution have the greatest priority. It is also desirable to accomplish steroscopic or three-dimensional viewing of the lunar surface and correlation of the mapping information with other experiments included in the vehicle. The VOIS package will be an integral part of a spacecraft designed for this mission. It will be the primary experiment associated with the spacecraft and, as a result, will dictate the requirements of the spacecraft in the areas of:

(a) Guidance and attitude control.

(b) Environmental control.

(c) Auxilliary power supply.

(d) Communications.

The major purpose of the study program under Contract No. 950005 is to determine the limitations of the selected system in accomplishing the desired mission while considering the constraints imposed upon the system by the interface requirements. At the initiation of the study program certain tolerances on the interface requirements were defined by JPL, and these are listed in Table I. In general, the study program is to be conducted in a parametric manner so that trade-offs between VOIS capabilities and interface requirements might be accomplished.

The study program conducted to date has been divided into separate sections corresponding to the major subsystem components. These areas are:

(a) Systems Analysis.

(b) Communications System.

(c) Electrostatic Tape Camera.

(d) Optical System.

The following sections of this interim report discuss the results of the study in each of these areas to date.

Table I

Preliminary System Characteristics

Orbital Characteristics	
Altitude (average)	100 to 500 km
Orbit Orientation	Polar, $\pm$ .1 degree
Circularity	1 to 10 percent
Payload Weight	300 to 500 pounds
Auxiliary Power	Several Hundred Watts
Attitude Stabilization	Local Vertical
Three-Axis Orientation	$\pm$ 0.1 degree
Angular Rates	0.01 to 0.1 degrees per hour
Transmission Characteristics	
Frequency	2300 megacycles
RF Bandwidth	$\pm$ 2 megacycles
Vehicle Antenna Gain	26 db
Ground Antenna Gain	50 db
System Noise Temperature	400^{o} Kelvin
Resolution	Highest obtainable (about 1 meter desired)
Lifetime	90 days

II. SYSTEMS ANALYSIS

A. INTRODUCTION

The system presently being studied consists of an electrostatic tape camera which scans the lunar surface in a panoramic manner and an S-band transmitter for relaying the images to the ground stations on earth. The camera is mounted at the image end of a telescope so that it can be rotated about the optical axis (Figure II-1). The optical image is projected on the electrostatic tape via a slit in the camera which is oriented at all times so that its longitudinal axis is normal to the image motion resulting from the motion of the vehicle and the scanning mirror (the mirror scanning in a direction normal to the motion of the vehicle). The electrostatic tape is moved past the slit so that its motion is synchronous with the image motion, thus producing on the tape a latent electrostatic image of the lunar surface. The tape speed is varied as a function of the average altitude of the vehicle in order to prevent relative motion between the image and the tape.

The quantity of electrostatic tape is sufficient for the storage of images obtained over several orbits, and the lunar surface is imaged on the tape at the highest resolution of which the system is capable. Separate guns are used for recording the image and for reading out the recorded image so that the system is capable of reading and writing simultaneously. In addition, several levels of resolution will be utilized on readout, with the highest level of readout at a resolution of 200 television lines per millimeter. A detailed discussion of the basic operating principles of the electrostatic tape and the camera design requirements is given in Section III. B.

B. BASIC SYSTEM PHILOSOPHY

In general, there are several areas of the VOIS experiment which will dictate some of the design choices for the system. The most desirable functions of the VOIS are to obtain high-resolution images of selected points on the lunar surface, and to map the entire surface of the moon not necessarily at the highest resolution capability of the system. In general, the resolution associated with the latter function will be limited by the transmission bandwidth of the communications system and by the fact that this mapping mission is to be accomplished in approximately 28.3 days (the time required for the moon to revolve once on its axis). It should be noted that most of the areas to be viewed at high resolution will not be known before obtaining the mapping data and that a long lead time would be desirable between obtaining the mapping information and the requirement for high-resolution viewing. However, there will be some areas for high-resolution viewing that will be known in advance, so the system should be flexible enough to

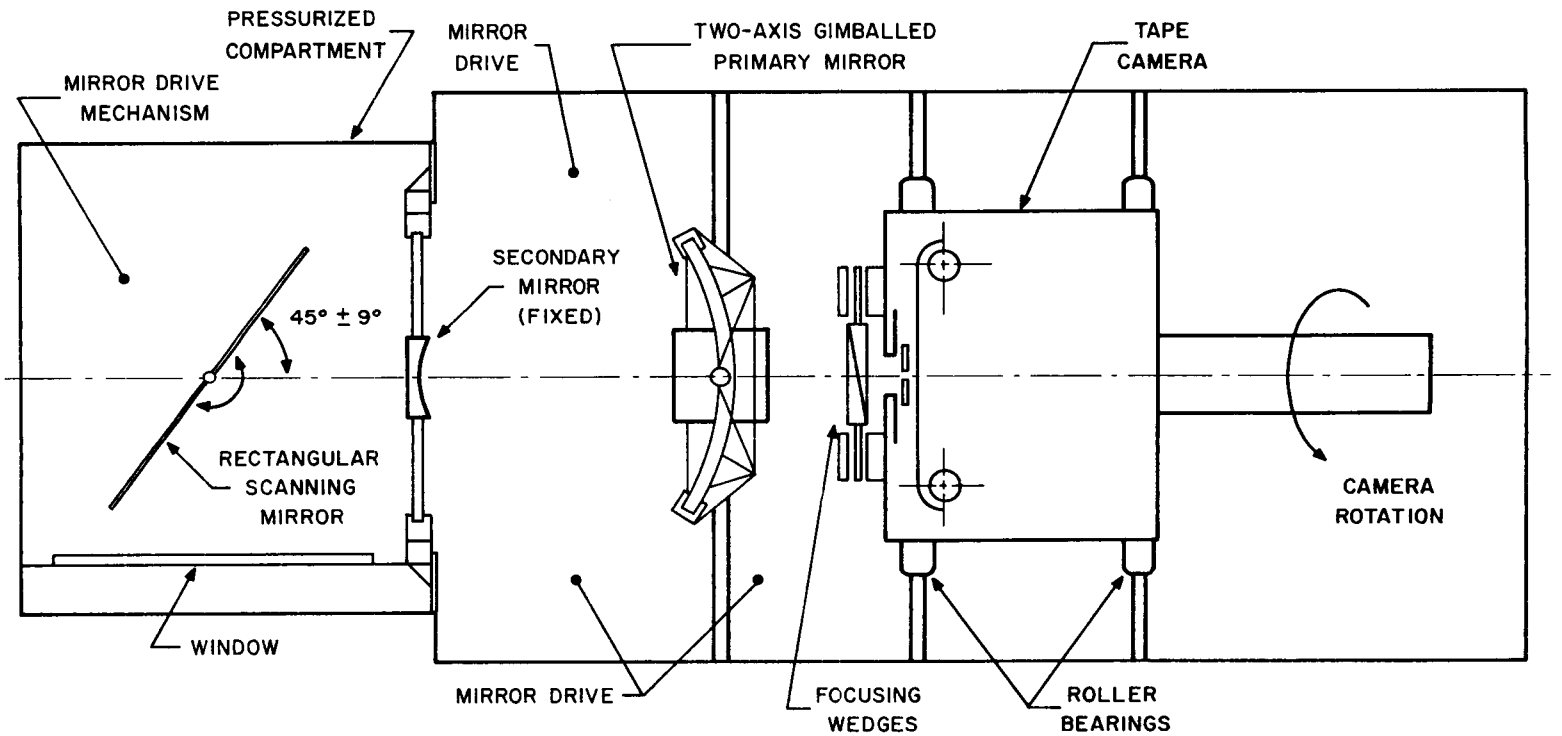

Figure II-1. Camera System Layout

accommodate high-resolution imaging and readout during the initial phase of the operation and to allow the mapping mission to be programmed simultaneously or at a later time in the operation.

One of the major problems associated with the high-resolution viewing of a selected lunar area is the directing or pointing of the optical axis at that area. With a limited field of view and with uncertainties in stabilization and orbital position, this problem could become insurmountable. One manner of circumventing this would be to image the entire surface of the moon over a 1-month period at the highest resolution capability of the system and to store this information within the vehicle. During each orbit of this 1-month period, data from the preceding orbit could be read out at a resolution consistent with the bandwidth of the transmission system and the transmission time available per orbit. This is accomplished while imaging the lunar surface for the given orbit. This process is possible if readout is not destructive. With an indexing system, the problem would thus be reduced to selecting those images that are to be read out from storage at high resolution after the 1-month period. The process presupposes a capability for reading out at different resolution levels. A disadvantage of the technique is the tremendous storage capacity required in the vehicle. The requirements are rather large for even such a high-density recording medium as electrostatic tape. Moreover, it would be wasteful to record such a quantity of data when only a relatively small amount is to be read out at high resolution.

Another method of recording and readout takes advantage of the same basic technique without requiring such large amounts of storage. Since the satellite will continue to orbit the moon and to view different areas of the lunar surface on each orbit, it is possible to continue the imaging of the lunar surface throughout the lifetime of the vehicle. If a limited amount of storage is available (for example, assume 10 orbits of storage capacity is available), then the moon can be mapped during a 1-month period with readout at the proper resolution on an orbit-to-orbit basis. Thus, 10 orbits of data could be stored in the vehicle at any given instant, and the image from the first stored orbit could be erased before imaging the eleventh orbit. In this manner, the decision for selecting a particular stored image for high-resolution readout could be delayed for 10 orbits from the time when the information was imaged on the tape.

It would not be advantageous, however, to continue reading the image information at the mapping resolution before selecting the high-resolution areas throughout the lifetime of the vehicle. The transmission time thus consumed by mapping-resolution readout would seriously limit the amount of high-resolution readout that could be accomplished. Therefore, a third and lower level of readout resolution is introduced to permit selection of areas for high-resolution readout. This level of pointing resolution is lower than that required for the mapping mission, so the time required to read out a given frame is also reduced. If the resolution were 10 times lower than the

mapping resolution, then the time required for readout at low resolution would be only one one-hundreth that required for the mapping mission. Since information imaged in one orbit is transmitted during one orbit for the mapping mission, only 1% of the transmission time per orbit would be consumed by low-resolution transmission and 99% would be available for high-resolution readout.

Some of the disadvantages of this method are that the addition of a third level of resolution increases the complexity of the camera equipment and that extending real-time readout over a period of up to 90 days subjects the system to an increased variation in the sun's position relative to the orbital plane. Over a period of 90 days, the sun angle would vary $\pm 45^{\circ}$, whereas it would vary $\pm 15^{\circ}$ during a 1-month period. The illumination of the lunar surfaces at the higher latitudes would thus be reduced during these extreme positions of the sun. The system flexibility offered by this method, however, could well outweigh these disadvantages.

Figure II-2 shows how readout could be programmed to allow for maximum high-resolution readout during the lifetime of the system. During the first 14 days, 99% of the time would be available for high-resolution readout of pre-programmed areas of interest, with only 1% of the time consumed by readout at the pointing resolution. During the succeeding 1-month period, 90% of the transmission time would be devoted to mapping-resolution readout and 10% of the time to high-resolution readout. For the remaining lifetime of the system, 99% of the time would again be devoted to high-resolution readout. In the particular case illustrated, the vehicle is initially injected into orbit so that the sun angle (angle between the sun's vector and the orbital plane) is -29°. Toward the end of the 90-day period, the sun angle becomes large enough to reduce significantly the latitudes where useful pictures can be obtained. A more symmetric splitting of the intervals could reduce this extreme condition.

With regard to the effect of high-resolution readout on the maximum resolution at which the entire lunar surface might be mapped in 1 month, consider the case where

t = time used for transmission of high-resolution data

T = total transmission time available

N = number of TV frames to be transmitted

n_v = number of TV lines in the vertical direction

n_h = number of TV lines in the horizontal direction and

B = bandwidth of the transmission system.

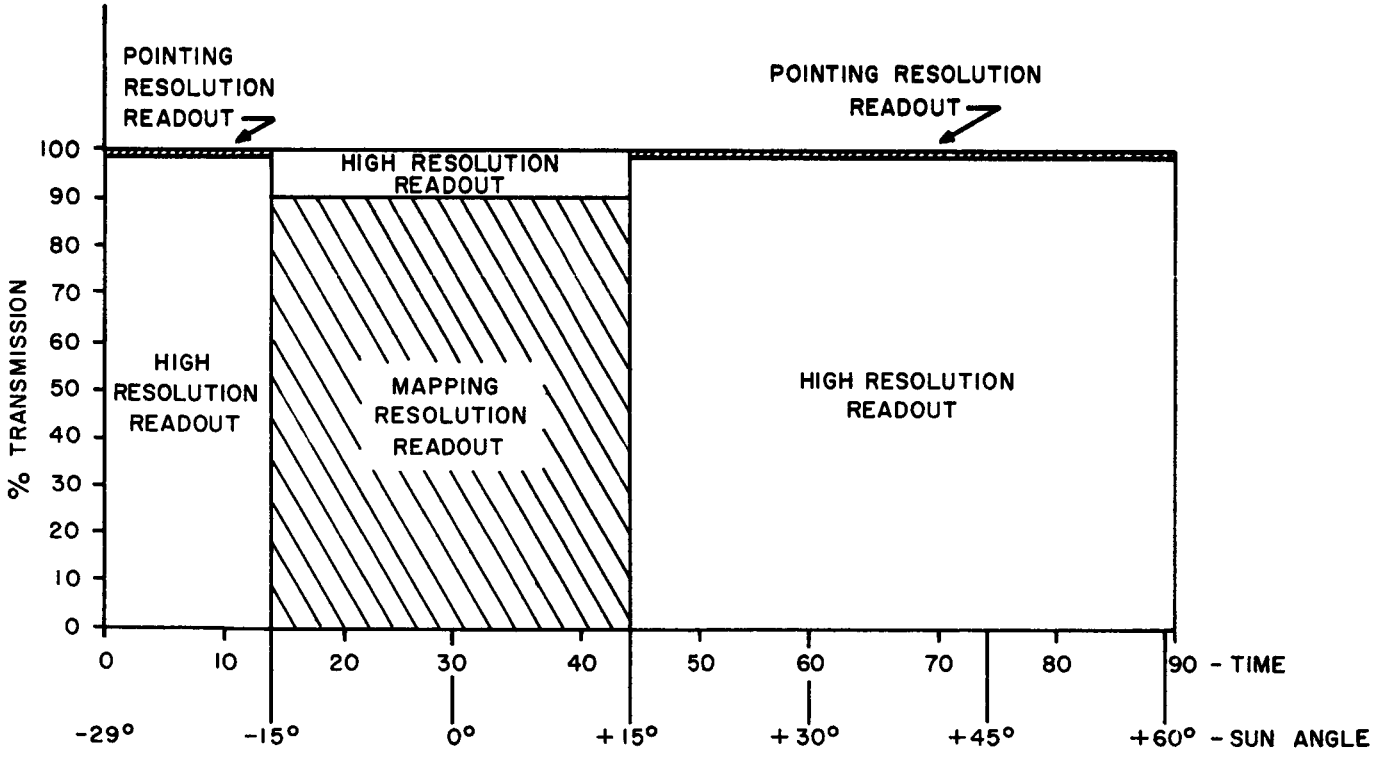

Figure II-2. Time Program of VOIS System

The number of elements, m, to be transmitted at the mapping resolution is given by

$$m = (n_v \cdot n_h) \text{ per frame.} \tag{II-1}$$

The number of cycles required of the transmission system per frame is m/2. The number of frames which can be transmitted is given by

$$N = 2(T - t)\ \frac{B}{m},$$

or

$$n_v \cdot n_h = \frac{2\ (T - t)\ B}{N} \quad . \tag{II-2}$$

For this analysis, no generality is lost in assuming $n_v = n_h = n$, and we have

$$n^2 = \frac{2\ (T - t)\ B}{N} \quad . \tag{II-3}$$

Now, if the information is imaged on the sensor such that the linear distance of the imaged lunar surface across the frame is x meters, then the resolution is given by

$$\delta = \frac{x}{n} = x \sqrt{\frac{N}{2\ (T - t)\ B}} \tag{II-4}$$

Letting

$$\delta_o = x \sqrt{\frac{N}{2\ (T)\ B}} \tag{II-5}$$

(i. e. no high-resolution readout), we obtain

$$\frac{\delta_o}{\delta} = \sqrt{1 - t/T} \quad . \tag{II-6}$$

This function is plotted for various values of percent transmission time for high resolution in Figure II-3. As can be seen from the figure, pointing

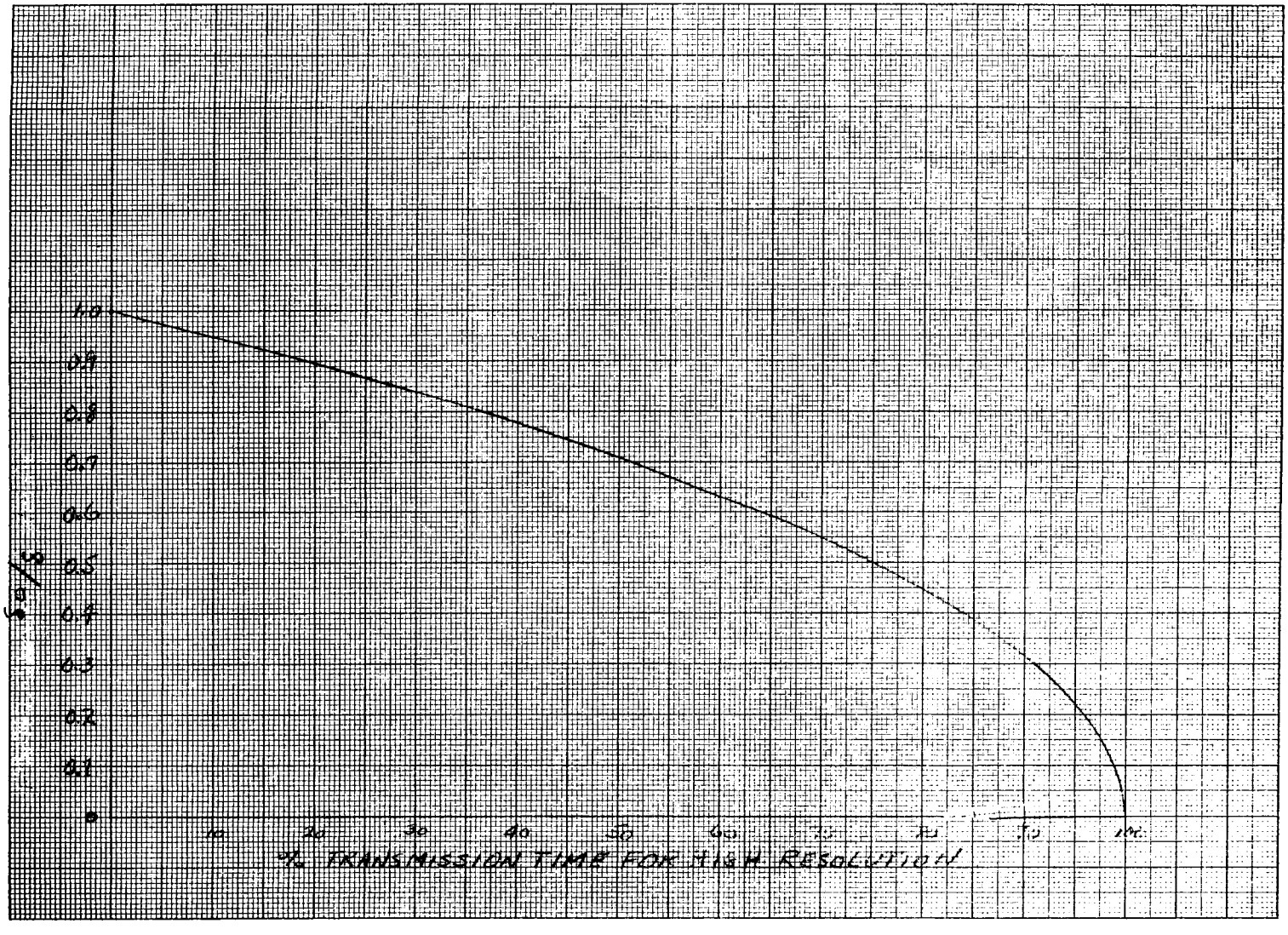

Figure II-3. δ_o/δ Versus Percent Transmission Time for High Resolution

resolutions degraded by only a factor of two over the maximum obtainable for the mapping mission will permit 75 percent of the time to be utilized for high-resolution readout.

One other point that should be discussed here is how the information might be utilized at the ground stations for selection of areas for high-resolution readout. During the initial phase of the operation, areas on the front face of the moon which can be seen from the earth might be selected before launch and be initially programmed so that each of the three DSIF stations could monitor the areas mapped on each orbit with a real-time display. The information read out at the pointing resolution could then be compared with previously prepared maps, and control points could be determined from which the indexing for selected areas to be read out at high resolution could be obtained. With a storage capability for 10 orbits, this would allow approximately 20 hours of lead time in initiating the high-resolution readout. After the mapping-mission interval, the areas selected for high-resolution readout could be derived by comparing the pointing resolution with the map obtained during this interval, thus, generating control points for the back face of the moon as well as for the front face. It should be pointed out that, throughout the whole operation, almost real-time data processing will be required, even though some lead time is available. This means a considerable problem in data processing on the earth.

C. ORBITAL CONSTRAINTS

The selection of the design criteria for the visual imaging instrumentation and the data storage, processing, and communications equipment will depend upon the altitude of the desired circular orbit and the attainable tolerances to this orbit. The range in orbital altitude to be considered during this study program is 100 to 500 kilometers, and the choice of altitude in this range will affect such parameters as: the required area to be scanned for each orbit so that complete coverage of the surface is obtained; the choice in aperture and focal length of the optical system for a given level of surface resolution; the time between frames or swaths for a panoramic system, and as a result the required tape speeds and scan rates; the image immobilization and exposure times; and the minimum transmission time available.

The characteristics of circular orbits in this altitude range have been analysed neglecting perturbations to the orbit, and are presented in Figure II-4. In addition, the effect of 10% circularity on the orbit is presented in Figure II-5. Of major importance with regard to the choice of orbital altitude is the requirement on the optical system for obtaining a given resolution. Considering the low levels of illumination that may be encountered near the lunar poles, it would be desirable to maintain a reasonably large light-gathering lens. Since the light-gathering properties are inversely proportional to the square of the ratio of focal length to diameter, it is desirable to maintain this ratio as low as possible. But considering the weight of a given lens, which varies approximately as the cube of the lens diameter, it would also be desirable to maintain reasonably small lenses. Thus, if a given weight is allowed for the optical system and a fixed focal-length-to-diameter ratio is maintained, the resolution will vary directly as the orbital altitude. In Figure II-6, the resolution obtainable from a 36-inch-focal-length lens having a focal-length-to-diameter ratio of 2.5 is shown. Also plotted in this figure is the scan angle normal to the orbit required for complete coverage of the lunar surface including a 10% overlap. This scan angle then defines the required field of view normal to the orbit. As can be seen from Figure II-6, a resolution of approximately 1 meter is obtained at an altitude of 200 kilometers. The field of view in the forward direction (parallel to the orbital plane) is defined by the image format size and the focal length of the lens. For a 36-inch lens and an active tape surface of 60 mm, this yields a field of view of 3° 45'. The rate at which each swath must be scanned will be a function of the velocity of the satellite over the lunar surface for a given optical system. Again with the 36-inch-focal-length lens and a 60-mm tape format, the time between swaths for circular orbits is shown in Figure II-7. A 10% overlap is included in these computations. Also plotted in this figure is the total number of swaths required per orbit considering one-half the circumference of the lunar surface being imaged per orbit. This does not take into account any reduction in imaging requirements caused by excessive overlap at the higher latitudes. In general, some savings in tape storage and transmission

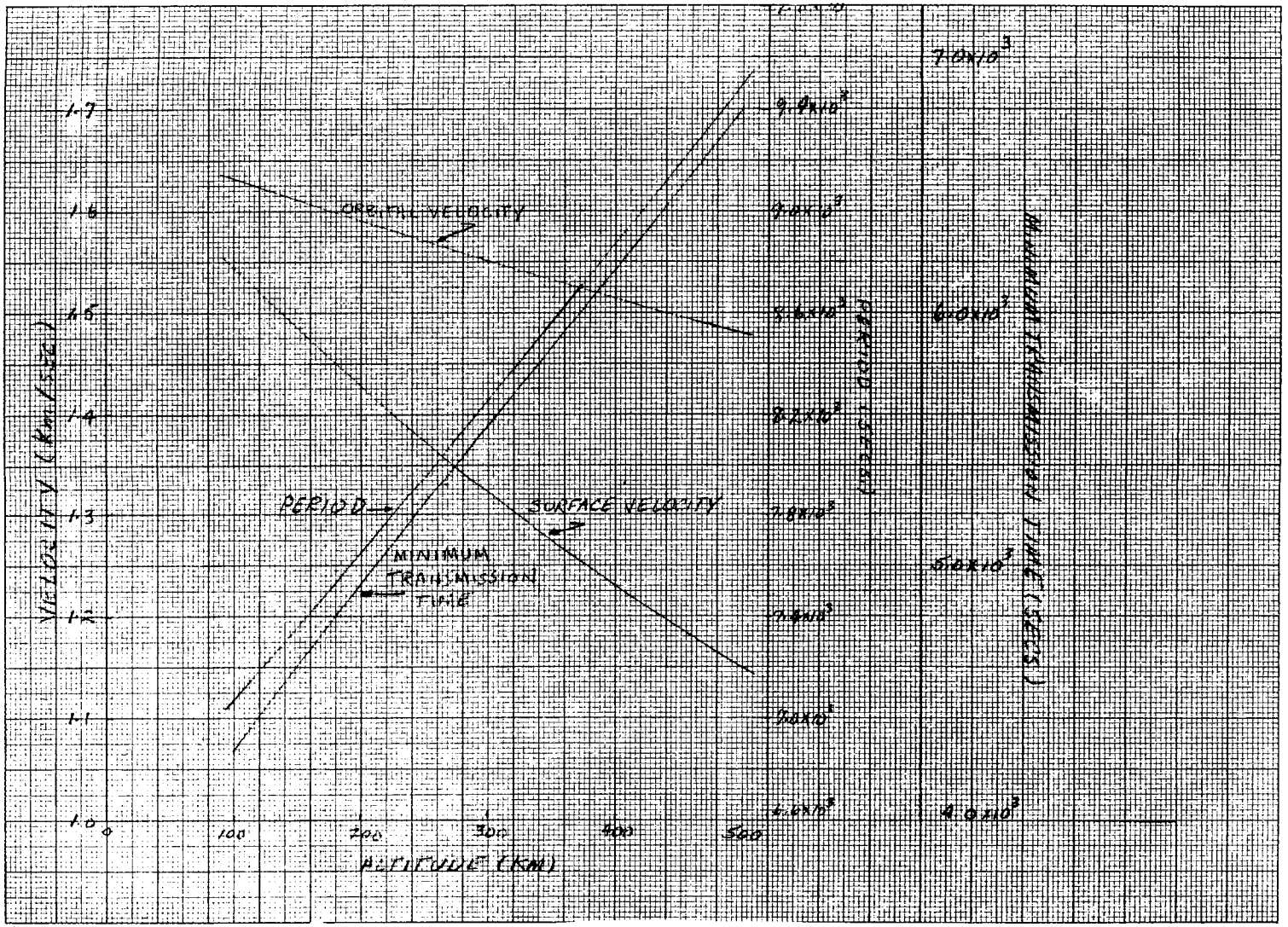

Figure II-4. Orbital Parameters for Circular Orbits

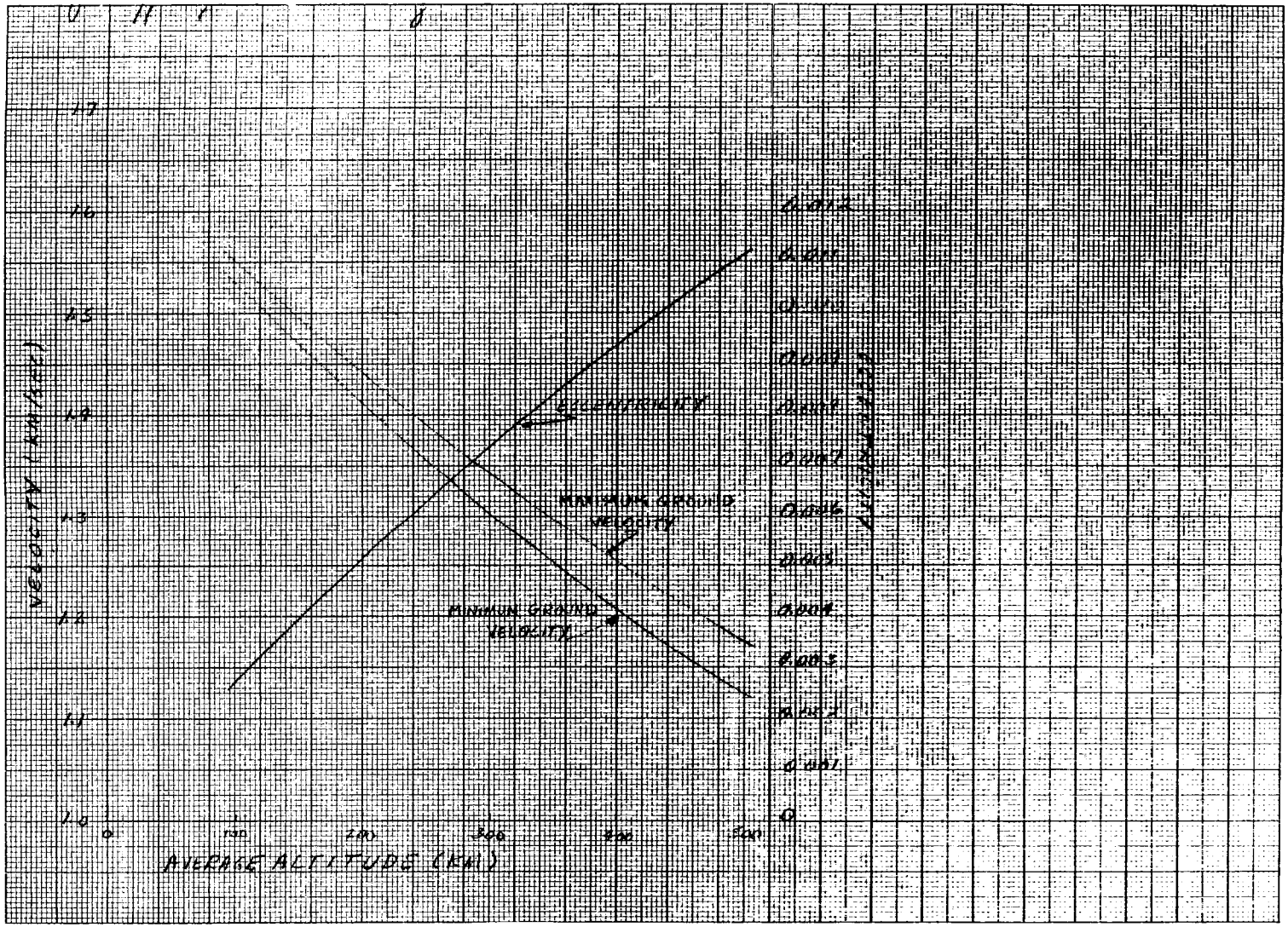

Figure II-5. Effect of 10% Circularity on Orbit

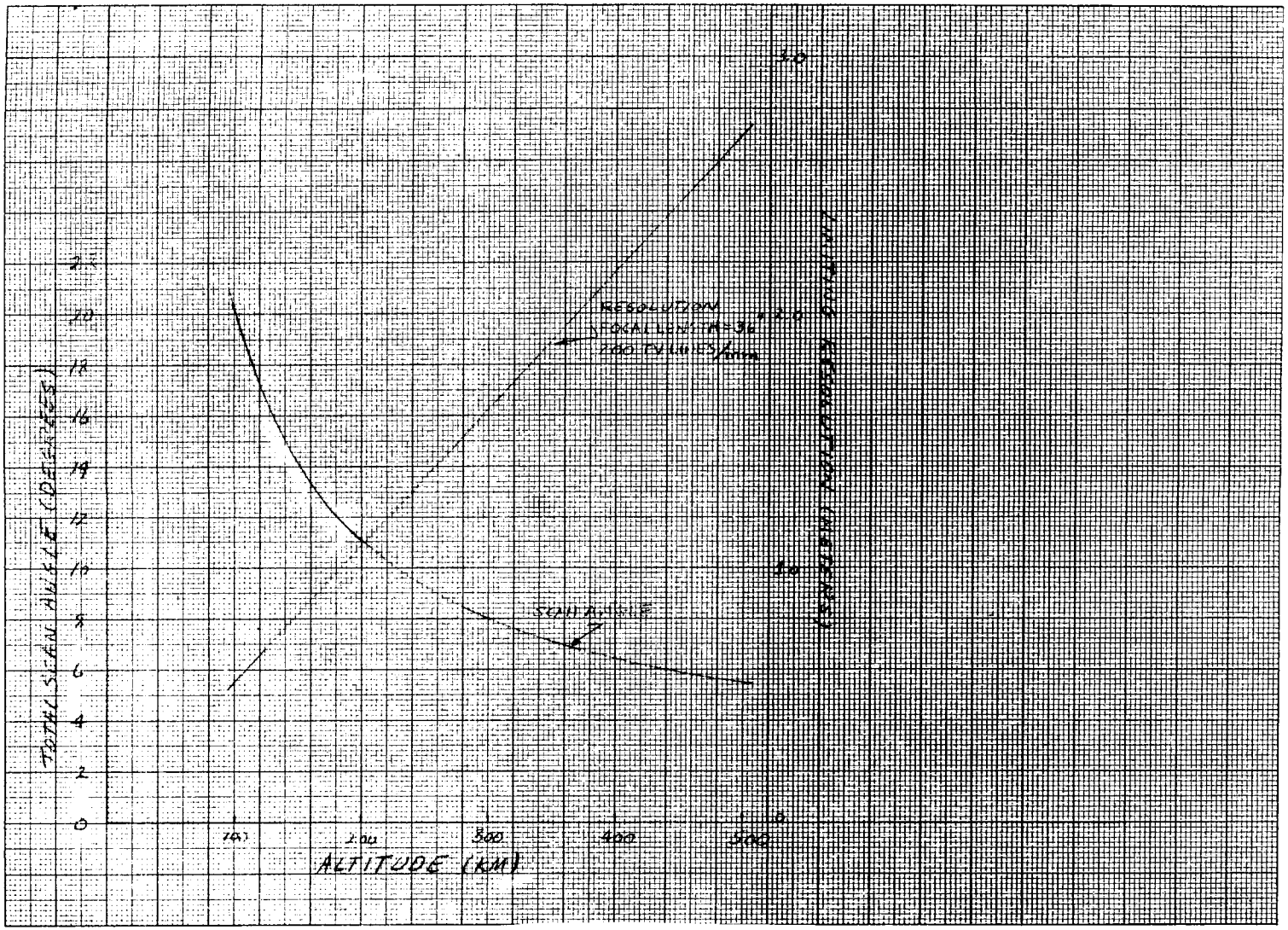

Figure II-6. Resolution and Scan Angle as a Function of Orbital Altitude

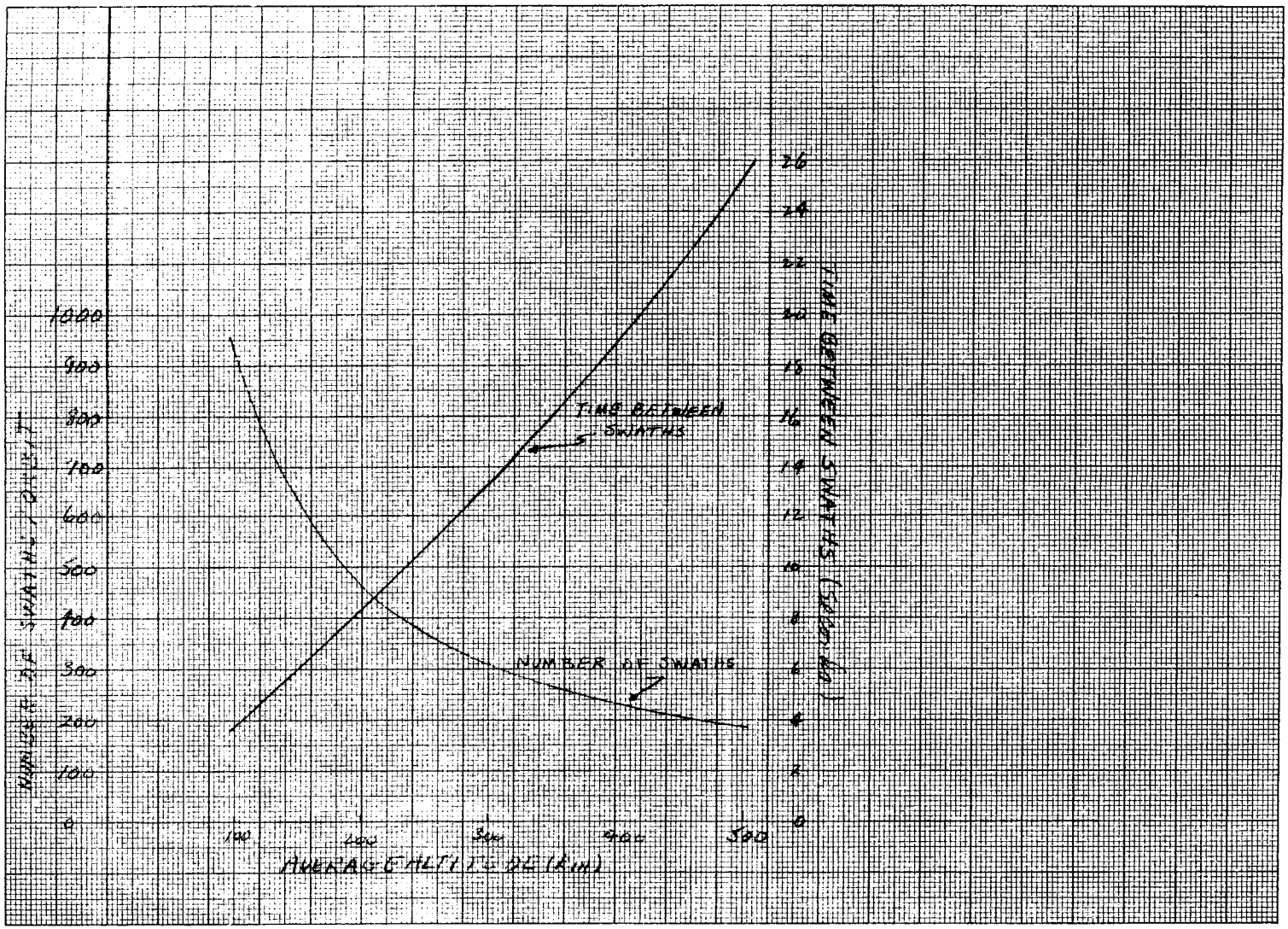

Figure II-7. Number of Scans and Time Between Scans Versus Altitude

bandwidth requirements could be achieved by not imaging the higher latitudes on every orbit. But it may be advantageous to obtain redundant data at the higher latitudes, since illumination levels will be lower in these regions and some stereoscopic presentation can be achieved where considerabe overlap in the swaths of successive orbits occurs. Furthermore, an estimate in the savings that could be achieved where the strip lengths are modulated to reduce redundancy is only 36%. This factor is not large enough to change the other system specifications to any great extent.

The video bandwidth of the system as given in Section III. A is approximately 500 kilocycles. Allowing a transmission time of 60% of the orbital period, the maximum resolution at which the entire lunar surface may be transmitted may be computed as a function of altitude. The bandwidth required for transmission of a given number of swaths is given by:

$$B = N \frac{n_v \cdot n_h}{2\,T} \qquad \text{(II-7)}$$

where B = bandwidth,

T = transmission time,

n_v = number of vertical lines,

n_h = number of horizontal lines, and

N = number of swaths to be transmitted.

Now, the ratio of n_h/n_v is a function of the forward field of view and the scan angle. Thus, Equation (II-7) may be written as:

$$B = Nk \frac{n_v^2}{2\,T}$$

where $k = n_h/n_v$,

$$\text{or } n_v = \sqrt{\frac{2\,TB}{Nk}} \qquad \text{(II-8)}$$

The maximum resolution, ξ_o, is obtained at n_v = 12,000 TV lines, which corresponds to a 60-mm tape format and 200 TV lines per mm. This resolution is given in Figure II-6 for a 36-inch-focal-length lens. Therefore, the maximum resolution at which the entire lunar surface may be mapped and transmitted in real time will be given by

$$\xi = \frac{12{,}000}{n} \quad \xi_o \tag{II-9}$$

This equation has been analyzed for a video bandwidth of 500 kilocycles and a transmission time of 60% of the orbital period, and the resolution with which the entire surface may be mapped and transmitted back in real time is approximately 7 meters/TV line and is independent of orbital altitude over the range from 100 to 500 kilometers.

D. SYSTEM CONSTRAINTS

1. Image Illumination

One of the major areas where difficulty will be encountered for this mission is in the variation of illumination levels of the lunar surface. First, the albedo of the moon's surface is small with a narrow dynamic range. For this study, the albedo model used is

$$R = 0.047 + 0.0136N, \tag{II-10}$$

where $0 \leq N \leq 10$.

The albedo is considered to be independent of wavelength and, for N = 0, corresponds to the blackest black and, for N = 10, corresponds to the whitest white. Thus, the dynamic range is approximately 3.5 to 1.

Secondly, the sun angle (i.e., the angle between the normal to the lunar surface being imaged and the sun's vector) will vary as a function of time and as a function of the latitude of the surface being viewed. Assuming that the sun moves in the moon's equatorial plane, the sun angle as a function of latitude is given by

$$\cos \phi = \cos \delta \cos \psi, \tag{II-11}$$

where ϕ = sun angle,

δ = latitude of surface being imaged, and

ψ = angle between the orbital plane and the sun's vector in the moon's equatorial plane.

Now, the relationship between image illumination, E_I, and object brightness, B_o, for objects at infinity is given by

$$E_I = \frac{T B_o}{4 (f/\#)^2} \quad \text{foot-candles}, \tag{II-12}$$

where B_o is in foot-lamberts;

T is the lens transmission factor, and

f/# is the focal-length-to-diameter ratio of the lens.

Also, if E_s is the incident illumination from the sun, ϕ is the sun angle of the object, and R is the albedo of the object, we have

$$B_o = RE_s \cos \phi \qquad \text{(II-13)}$$

Figure II-8 is a plot of the image illumination, assuming E_s = 13,000 foot-candles, f/# = 2.5 and T = 60%. The illumination level is plotted for the two extreme values of R obtained from Equation (II-10) and for various positions of the sun with respect to the orbital plane at the moon's equator. Also shown in this plot are the minimum illumination levels for the present and future predicted capabilities of the electrostatic tape. In both cases, a 4-millisecond exposure time was used. As can be seen from the figure, up to latitudes of about 85° sufficient illumination is available even for extreme sun angles.

2. Exposure Time and Image Immobilization

For the present system utilizing a slit-type camera and a panoramic scan of the lunar surface, image immobilization is obtained by pulling the tape past the slit in such a manner that the velocity of the tape exactly compensates for the image motion. The image motion will have two major components. The motion of the satellite over the lunar surface will produce a relative motion parallel to the orbit of any point on the surface. In addition the motion generated by the scanning mirror will also produce a relative motion in the image plane, and its direction is normal to the orbit. The image motion produced by the motion of the satellite over the lunar surface will be affected by

a. Orbital speed and altitude.

b. Maximum field of view normal to and parallel to the orbit.

c. Moon's rotation.

d. Yaw angles of the satellite.

Consider the geometry shown in Figure II-9. The velocity of any point in the object plane resulting from motion of the satellite will be given by

$$V = V_S \cos P,$$

where V is normal to r_2 and in the plane defined by r_1 and r_2.

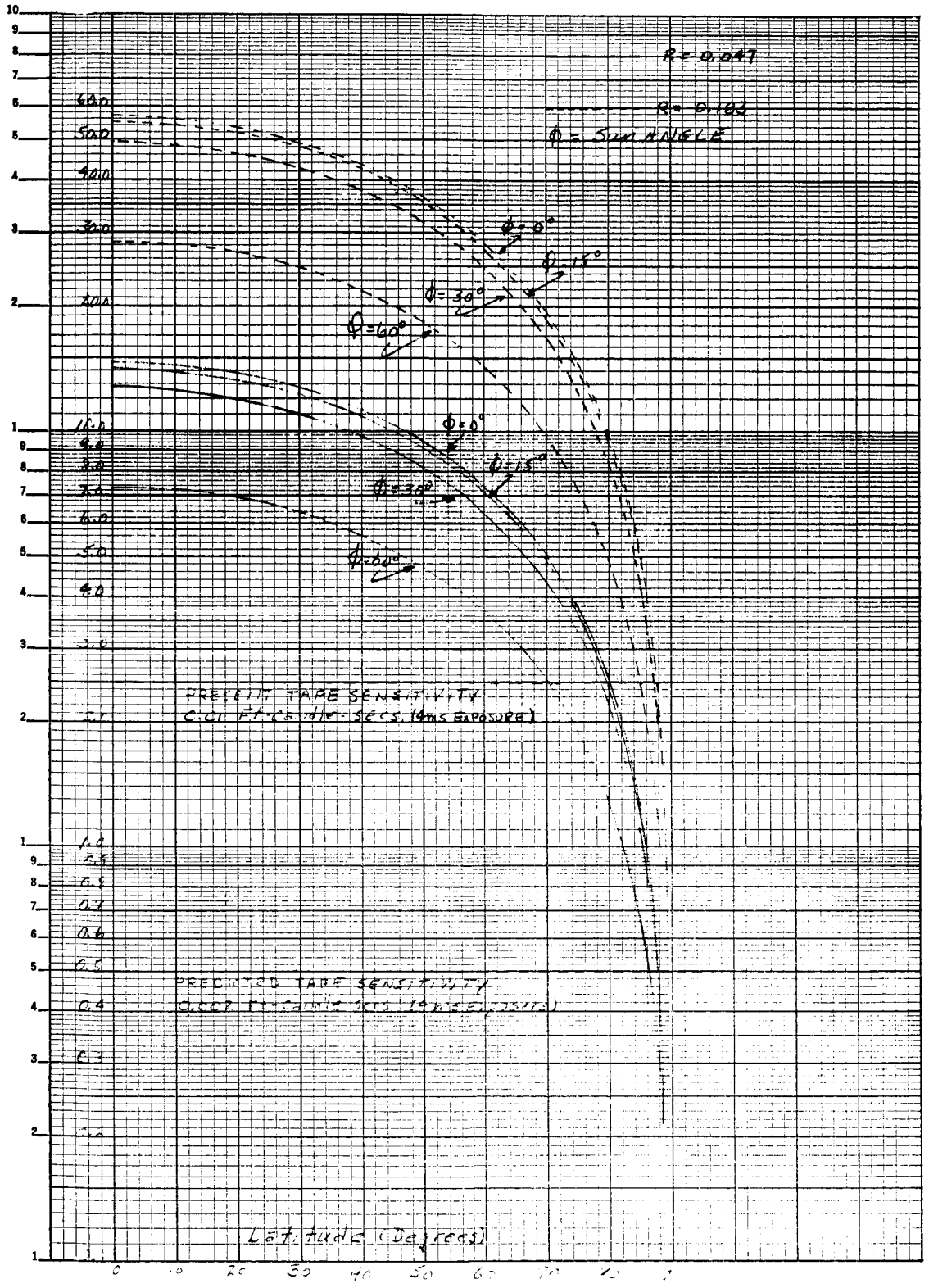

Figure II-8. Image Illumination Versus Object Latitude and Sun Angle

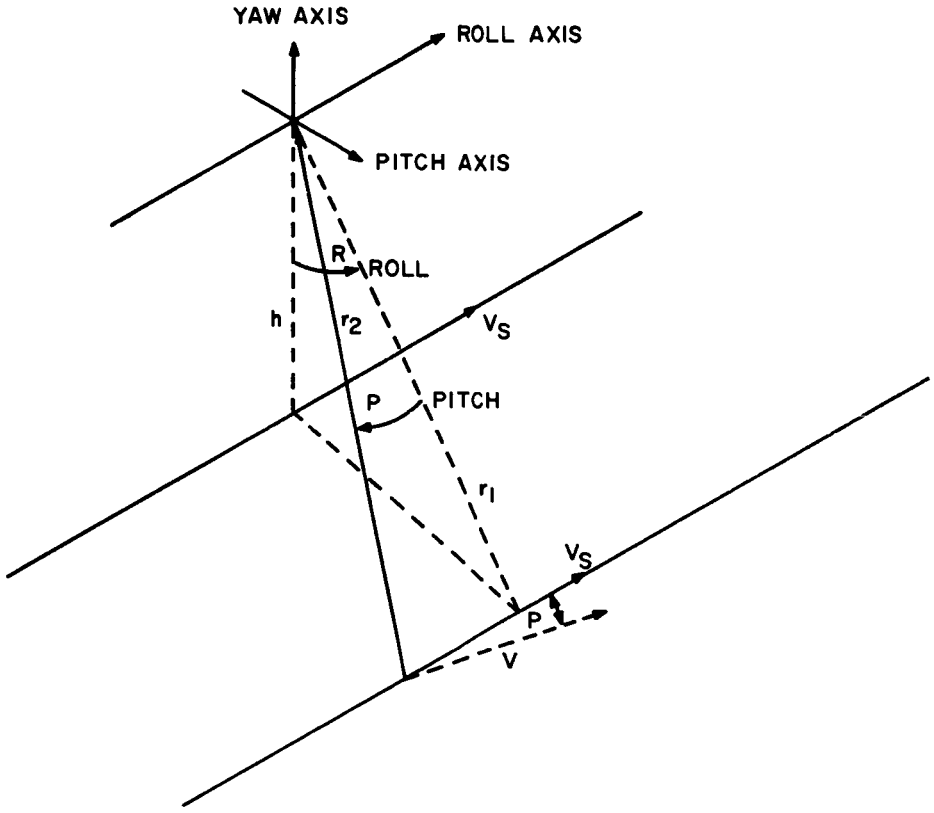

Figure II-9. . Image - Motion Geometry

Furthermore,

$$r_2 = r_1/\cos P$$

$$\text{and } r_1 = h/\cos R \qquad \text{(II-13)}$$

Thus,

$$r_2 = \frac{h}{\cos P \cos R}$$

Now, defining ω_i' as the image angular velocity resulting from satellite motion, we have

$$\omega_i' = \frac{V}{n_2} = \frac{V_g}{h} \cos^2 P \cos R. \qquad \text{(II-14)}$$

Since the image angular velocity at the nadir, ω_o, is given by

$$\omega_o = \frac{V_g}{h}, \qquad \text{(II-15)}$$

we obtain

$$\omega_i' = \omega_o \cos^2 P \cos R$$

The maximum image angular velocity parallel to the orbit occurs at the nadir, and the minimum angular velocity occurs at the extremes of the scanned area. Figure II-10 shows a plot of ω_i'/ω_o as a function of roll angle and pitch angle. For the case of a 36-inch-focal-length system and the 70-mm tape format and a 200-km orbit, the maximum roll angle (scan angle) is approximately ± 5.5 degress and the maximum pitch angle is approximately ± 1.9 degrees. Thus the maximum variation in ω_i'/ω_o is from 0.994 to 1.0, or approximately 0.6%. Figure II-11 shows a plot of ω_o as a function of altitude.

The motion generated by the scanning mirror will be a function of the time between swaths and the scanning angle required. Both of these parameters are functions of the altitude and are shown in Figures II-7 and II-6, respectively. Since the rotating mirror will be designed to scan the orbit always in a given direction, time will have to be allowed for flyback of the mirror. Assuming the flyback speed to be three times the scanning speed, then the time available for scanning will be 67% of the total time between swaths. For a 200-km orbit, then, the image angular motion ω_i'' produced by the scanning mirror is approximately 0.037 radian/sec. Thus, it is proposed to pull the tape past the slit at a constant speed, $\overline{\omega_i}$, and rotate the camera through an angle η with respect to the forward motion of the vehicle, the two velocity components of the tape compensating for the total image motion. The equivalent tape angular velocity is:

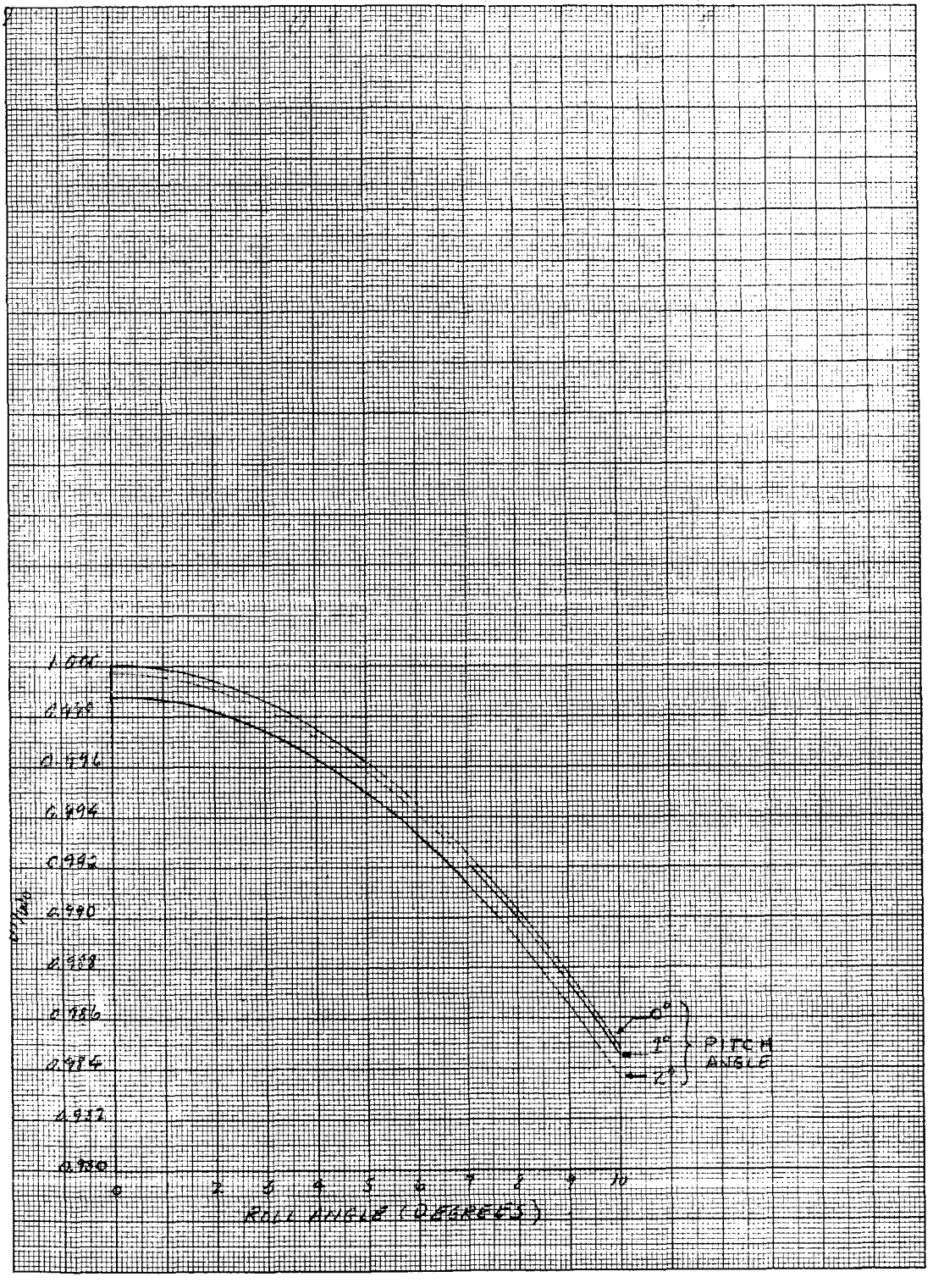

Figure II-10. Angular Velocity of Image as a Function of Pitch and Roll Angles

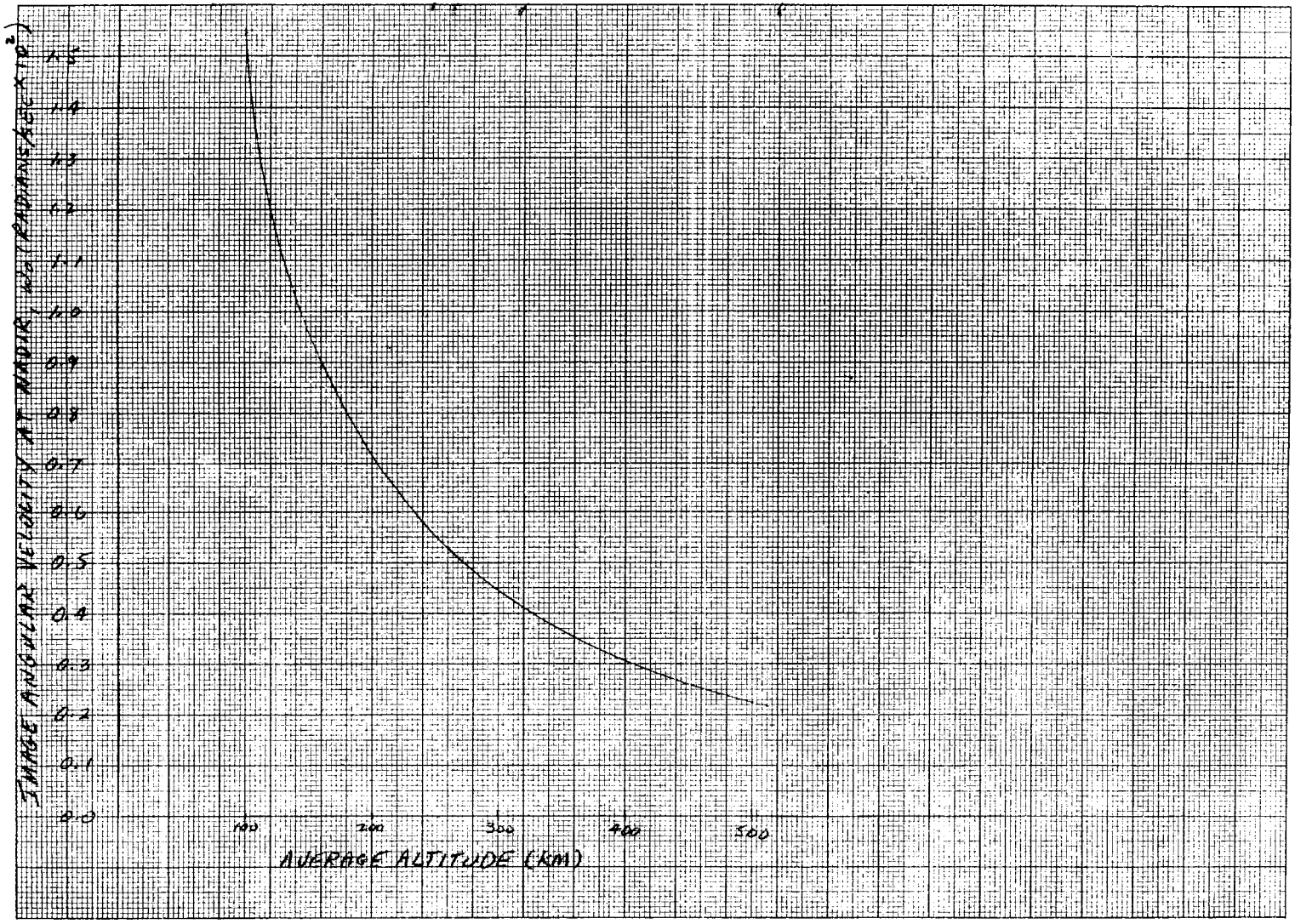

Figure II-11. Angular Velocity of Image as a Function of Altitude

$$\overline{\omega_i}^2 = (\omega_i')^2 + (\omega_i'')^2, \qquad \text{(II-16)}$$

and

$$\tan \eta = \frac{\omega_i'}{\omega_i''} \qquad \text{(II-17)}$$

For a 200-km orbit and the same optical and tape format previously discussed, we have

$$\overline{\omega_i}^2 = (0.0071)^2 + (0.037)^2.$$

or

$$\overline{\omega_i} = 3.77 \times 10^{-2} \text{ rad/sec}$$

and

$$\eta = 10.86 \text{ degrees},$$

where

$$\omega_i' = 0.997\, \omega_o = 0.71 \times 10^{-2} \text{ rad/sec}$$

$$\omega_i'' = 3.7 \times 10^{-2} \text{ rad/sec.}$$

Since an object of 1.1 meters at 200 km subtends an angle of 5.5×10^{-6} radians, corresponding to a distance on the electrostatic tape of 5×10^{-3} mm for 200 TV lines/mm, the linear tape speed is given by

$$V_T = \frac{3.77 \times 10^{-2} \times 5 \times 10^{-3}}{5.5 \times 10^{-6}} = 34.2 \text{ mm/sec}$$

In order to determine the exposure time and, as a result, the slit width, it is necessary to determine the maximum allowable error in image-motion compensation for the system. If it is required that the image misalignment be less than one-quarter the separation between TV lines during the exposure time, t. The component of image angular velocity causing smear then, for the previous case, will be

$$\Delta\omega_i = \frac{5.5 \times 10^{-6} \text{ radians}}{4 \text{ (exposure time)}}$$

If F is the fractional error in angular velocity and t is the exposure time, then

$$\Delta\omega_i = F\,\omega_i = \frac{5.5 \times 10^{-6}}{4\,t},$$

or

$$tF = \frac{5.5 \times 10^{-6}}{4\,\omega_i}$$

Allowing a 1% vector error in image motion (i.e., F = 0.01) and taking the maximum image motion, then

$$t = \frac{5.5 \times 10^{-6}}{4 \cdot (3.77 \times 10^{-2})} = 3.66 \text{ milliseconds.}$$

In general, it is expected that the error in image-motion compensation can be kept less than this so that a 4 millisecond exposure time will be possible. The slit width ΔX for this particular case can be computed from

$$\Delta X = V_T t = 34.2 \times 4 \times 10^{-3} = 0.137 \text{ mm}$$

which is well above the diffraction limitation of the slit.

III. COMPONENT ANALYSIS

A. COMMUNICATION SYSTEM

1. Introduction

The satellite transmitting equipment, which includes the transmitter, modulating equipment, encoder, and any special power supply peculiar to these components competes directly with the VOIS package for space, weight, and primary power. Thus, any optimization of the VOIS package must consider the satellite transmitter. The satellite transmitter, in turn, has a form strongly dependent on the earth-bound communication system and the specific techniques employed.

The purpose of the following discussion will be to define the more important problems of the communication system as they are now understood so that a proper optimizing procedure can begin. Modulation techniques, transmitter tube capabilities, weight, efficiency, and reliability will be considered, as well as the Deep-Space Instrumentation Facility (DSIF) (projected to 1964).

2. Transmitter Modulation Techniques

The theoretical channel capacity of a communication system has been shown by Shannon to be:

$$I = B \log_2 (1 + \overline{P}) \text{ bits per second,} \qquad \text{(III-1)}$$

where B = bandwidth and

$\overline{P}$ = ratio of average signal power to average noise power.

The equation shows that bandwidth may be traded for transmitter power, or vice versa, for a given rate of transmission. For the particular experiment under study and considering the finite lifetime and the maximum weight limitations of the vehicle, the optimum transmitter should approach minimal power (achieved at the expense of RF bandwidth) consistent with good system reliability and compatibility with the DSIF. The efficiency with which the trade-off of RF bandwidth versus RF power takes place depends strongly upon the modulating technique.

The modulating techniques of interest for this experiment are:

(a) Straight FM system.

(b) Straight FM system with frequency compression (Chaffee feedback) and/or phase-lock demodulation.

(c) Pulse code transmission (PCM).

(d) PCM with orthogonal coding (digilock).

a. Straight FM System

Considering a uniform energy modulating spectrum, the output signal-to-noise ratio (rms/rms) for an FM receiver is

$$S/N = \sqrt{3}\ (C/N)\ \delta \sqrt{\frac{B}{2b}}, \qquad \text{(III-2)}$$

where S/N = output signal-to-noise ratio (rms/rms),

C/N = input carrier-to-noise ratio (rms/rms),

δ = modulation index = f_d/b,

b = baseband (video bandwidth),

f_d = one-half the peak-to-peak deviation, and

B = RF or IF bandwidth.

Assuming that all side bands which are less than 10% of the unmodulated carrier can be neglected, then Equation (III-2) can be written as

$$S/N = \sqrt{3}\ (C/N)\ \delta \sqrt{1 + \delta}. \qquad \text{(III-3)}$$

Examination of Equation (III-3) reveals the FM improvement factor. For a constant output signal-to-noise ratio, the required input carrier-to-noise ratio can be decreased for an increasing modulation index. Unfortunately, there is a minimum value of (C/N) below which Equation (III-3) is no longer valid, where the output signal-to-noise ratio decreases far more rapidly than does the input signal-to-noise ratio. This value of C/N is called the improvement threshold. For conventional FM receivers, the improvement threshold is about 12 db. However, with good limiter design and adequate maintenance, the receiver improvement threshold can be reduced to about 10 db.

For Gaussian (thermal) noise distribution, the noise power N is

$$N = KTB = 2KTb(1 + \delta), \qquad \text{(III-4)}$$

where K = Boltzmann's constant,

T = effective absolute temperature of system,

and the required receiver power, P_r, is

$$P_r = (C/N)^2 \quad KT\,(1 + \delta\,)\,2b. \qquad \text{(III-5)}$$

Once the required baseband and equivalent system noise temperature are known, the required power at the receiver input terminals can be calculated from Equation (III-5). There is an optimum value of the modulating index δ which gives the minimum P_r for a given output signal-to-noise ratio. This value is obtained by solving Equation (III-3), assuming a realistic receiver improvement threshold. Values of δ less than the optimum value increase (C/N) for a given (S/N); values of δ more than the optimum value only increase the noise bandwidth, since C/N is already at the minimum value because of threshold. An example of this is shown in Figure III-1 for the given set of conditions listed. Note that the required transmitter power has a broad but definite minimum in the vicinity of the optimum modulation index.

For the purpose of comparing different modulation techniques, a standard set of conditions will be assumed. Using Equations (III-2) through (III-5) and assuming the following conditions, the required receiver carrier power may be calculated:

b = 100 kc,

C/N = 10 db,

B = 550 kc,

δ = 1.75

T = 400°K, and

P_r = -135.2 dbw.

The noise bandwidth of the receiver must be limited to B; otherwise, the increased noise power will decrease the receiver sensitivity. This implies that there is also an optimum IF bandwidth for the conditions assumed, which stems from the improvement threshold characteristic of the FM receiver. The improvement threshold in an FM system limits the extent to which bandwidth may be traded for transmitter power (for maximum sensitivity).

b. Straight FM System with Frequency Compression or Phase-Lock Demodulator

There are two methods currently used to reduce the improvement threshold in FM receivers. One of these methods, known as FM with

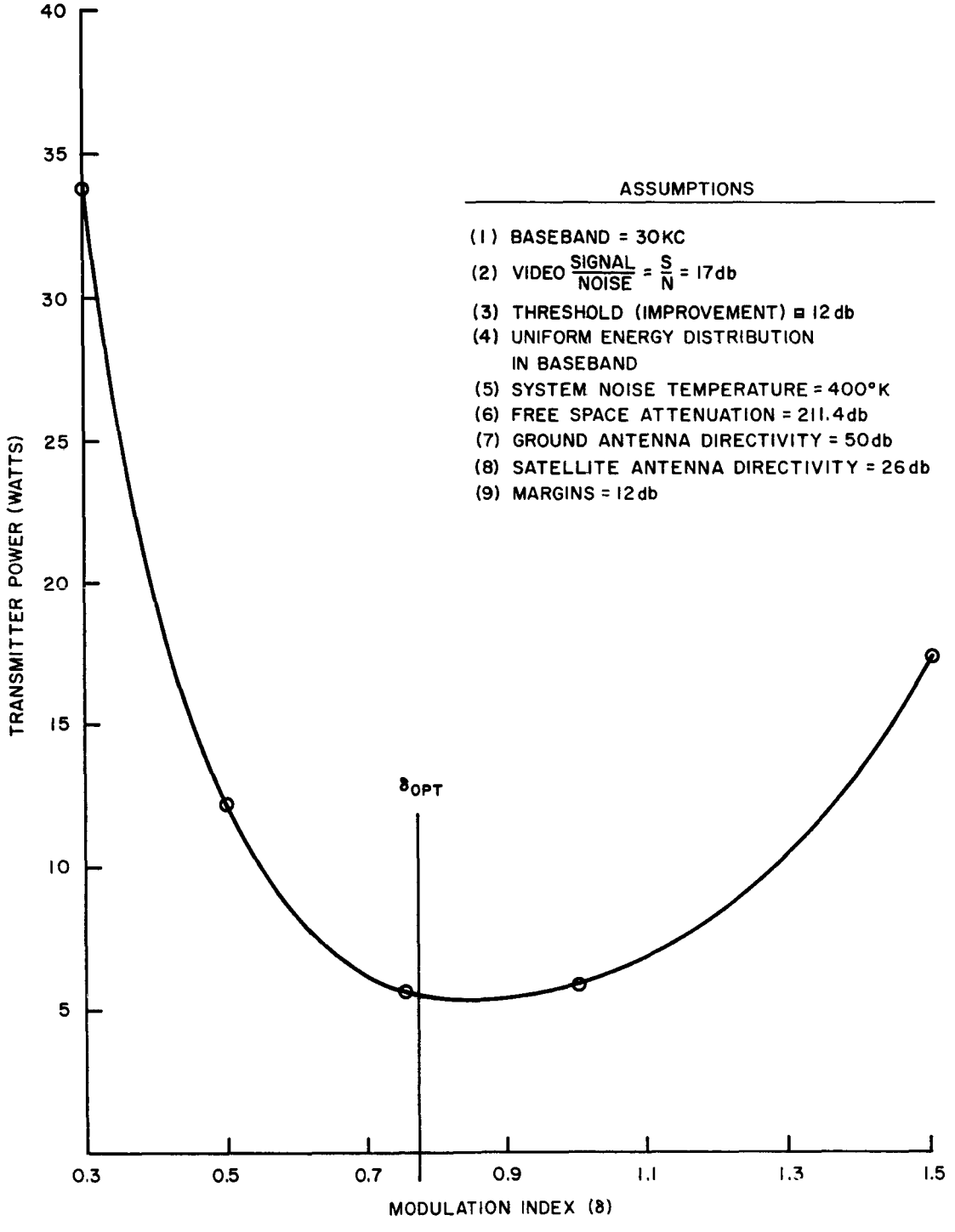

Figure III-1. Transmitter Power Versus Modulation Index (That Power Necessary for Minimum Threshold of 12db)

feedback (FMFB) or frequency compression and first proposed by Chaffee*, uses the discriminator output to frequency-modulate the receiver local oscillator as shown in Figure (III-2). It can be shown that frequency compression modifies Equation (III-5) to:

$$P_r = (C/N)^2 \, KT \left(1 + \frac{\delta}{1 + \mu}\right) 2b, \qquad \text{(III-6)}$$

where μ = feedback-loop gain.

Equation (III-6) can be rewritten as

$$P_r = \left\{ (C/N)^2 \left(\frac{1 + \frac{\delta}{1 + \mu}}{1 + \delta} \right) \right\} KT \, (1 + \delta) \, 2b. \qquad \text{(III-7)}$$

The bracketed term can be identified with a new receiver improvement threshold reduced from its former value by the ratio of the compressed IF bandwidth to the uncompressed IF bandwidth. The new receiver improvement threshold may be considered as the equivalent carrier threshold, provided that the RF bandwidth and IF bandwidth are the same. Considering reasonable values of δ and μ, the improvement threshold of the receiver can be reduced to about 6 db.

Equation (III-1) has been used to calculate the approximate efficiency of the FMFB system. If efficiency is defined as the ratio of the number of bits transmitted to the number of bits which could theoretically be transmitted through the medium for a given signal-to-noise ratio, then the efficiency of the FMFB is of the order of 15 to 20% for the conditions equivalent to a 6-db threshold.

The FMFB system will fail to operate when the noise in the loop becomes excessive; that is, when the local oscillator will not lock on. This system defect is also that of the phase-lock demodulator, for which the problems of acquisition and synchronism have been studied to a greater extent. One might expect then that the two methods would yield comparable results in practice.

A block diagram of a phase-lock demodulator is shown in Figure (III-3). B. D. Martin* has shown that, for a coherence phase range of 90°, the

* J. G. Chaffee, "The Application of Negative Feedback to Frequency Modulation Systems," Proceedings of the IRE, Vol. 27, May 1939.

* B. D. Martin, "Threshold Improvement in an FM Subcarrier System," March 1960.

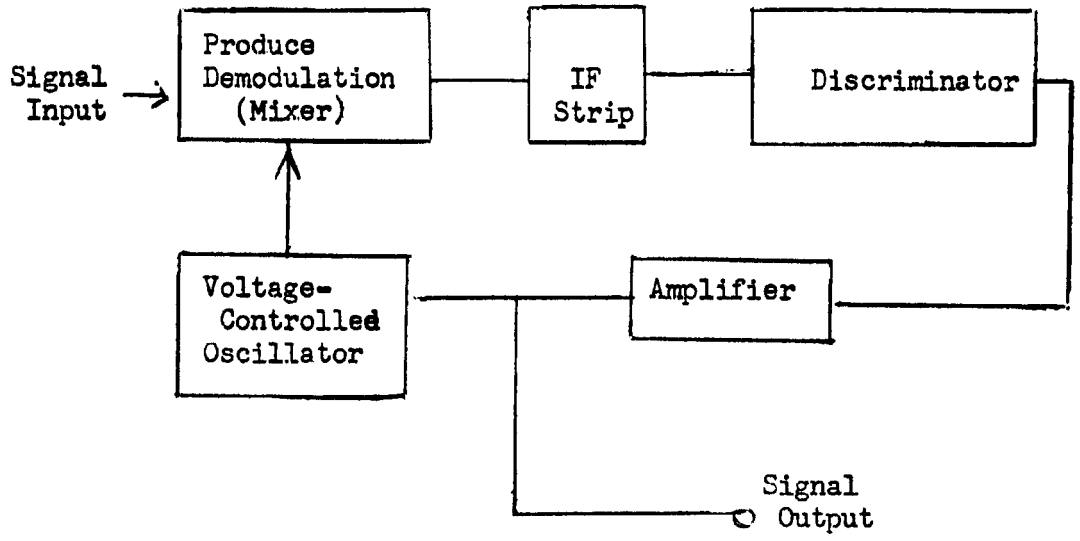

Figure III-2. Block Diagram of Chaffee Receiver with Negative Feedback

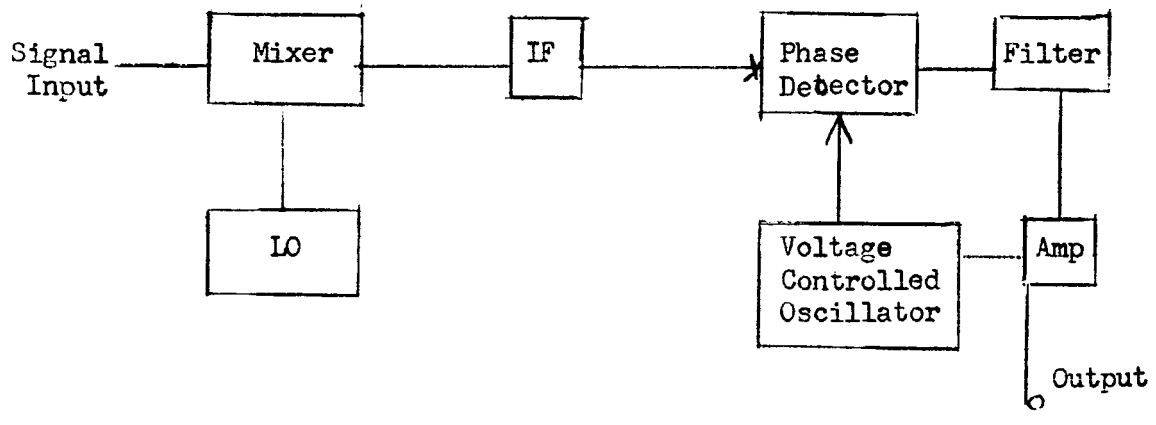

Figure III-3. Block Diagram of Phase-Lock Demodulator

theoretical equivalent improvement threshold is 4.5 db at the point where the output signal just begins to degrade because of lack of synchronism (0.26% error), considering reasonable phase nonlinearities. Practical values of equivalent improvement threshold are about 6 db*, and these values have been reported by others.

Using the 6-db threshold, the following conditions may be calculated for either FMFB or phase lock:

b = 100 kc,

C/N = 6 db,

B = 700 kc,

δ = 2.5,

T = 400°K, and

P_r = -138.1 dbw, or an improvement of about 3 db over the straight case.

The reduction in transmitter power of 3 db represents a substantial improvement in system performance when it is realized that this improvement is achieved at no increase in the complexity of the satellite equipment. The selection of either FMFB or phase lock will probably depend on practical problems in design and/or compatibility with DSIF equipment.

c. FM-FM

The use of a subcarrier frequency for FM is a technique widely used in telemetry. It is apparent, however, that the subcarrier frequency, which carries no information, must occupy a portion of the total RF spectrum. Therefore, the efficiency of a subcarrier system will always be less than that of a straight FM system. Other system requirements may require its use, as for instance magnetic tape storage, which requires a subcarrier. The electrostatic tape storage technique does not require a subcarrier.

d. Pulse Code Modulation (PCM)

Pulse code modulation is a technique whereby the amplitude of the modulating waveform is sampled periodically and converted into a pulse code. After transmission through the medium, the code is detected and converted back to its original form. PCM has certain advantages in relay communications systems in that the signal may be handled by any number of intermediate relay stations. If the noise level of every part of the system is below a certain finite level, the original signal is not altered by noise.

Let us consider a specific example of a PCM system with uniform energy density over the baseband with all filters ideal. For a maximum modulating frequency of 100 kc, a theoretical sampling rate of 200 kc is required. A 32-level PCM system (with five bits per sample) requires a minimum baseband of 500 kc and an RF bandwidth of 1 mc.

The maximum quantizing error for a 32-level PCM system is 1/64 of the peak-to-peak signal. A probability of error of 0.01 can then be assumed, since there is no point in operating at a carrier-to-noise ratio such that the error rate caused by noise is very much less than quantizing noise.

The bit error is 0.002 for a word error of 0.01, so that the required carrier-to-noise ratio may be computed from the probability function

$$P(x) = \frac{1}{v\,2\,\pi} \int_{x}^{\infty} e^{\frac{-x2}{2}}\, dx \qquad \text{(III-8)}$$

The variable x is the ratio of the peak voltage level to the rms noise level. For P (x) = 0.002, x = 2.88 = 6.2-db rms-carrier-to-rms-noise ratio. We should also allow for certain imperfections in the decoding apparatus which lead to additional losses of several db. However, since we are treating an idealized case, these imperfections are ignored. The following table results:

b = 500 kc,

C/N = 6.2 db,

B = 1 mc,

T = 400°K,

f_m = 100 kc, and

P_r = 136.4 dbw.

e. Orthogonal Coding

Additional savings in transmitted power can be realized by the use of special encoding techniques, such as "digilock". A 16-bit word would be required for a 32-level code transmission using a Reed-Muller, or modified Reed-Muller, encoding process. A system sensitivity improvement of 4 to 6 db over PCM has been reported for orthogonal systems.* Assuming the more optimistic value, the following results:

* R. W. Sanders, "Communication Efficiency Comparison of Several Communication Systems", Proceedings of the IRE, April 1960, pp. 575-588.

b = 1.6 mc,

B = 3.2 mc,

T = 400°K,

f_m = 100 kc, and

P_r = -142.4 dbm.

A comparison of the various modulation systems is as follows:

Modulation	Receiver Carrier Power (dbw)	Bandwidth (kc)
FM	-135.2	550
FMFB or phase lock	-138.1	700
PCM	-136.4	1000
Orthogonal PCM	-142.4	3200

The more important factors considered in comparing the above modulation systems are:

(1) Minimum transmitter power.

(2) Reliability.

(3) Weight, efficiency, size, and complexity.

(4) Compatibility with ground equipment.

On this basis, PCM should be discarded because it requires considerable power and special encoding apparatus on the vehicle, thus decreasing reliability. FMFB, on the other hand, needs less power than does an FM system and does not require an increase in vehicle equipment. Thus, the choice remains between FMFB (or phase lock) and orthogonal PCM.

A more critical examination of the comparison factors listed above leads to the conclusion that FMFB or phase lock is the better choice. First, it is believed that the 4.3 db less power required in the orthogonal coding system is more than offset by the loss of reliability in the intricate encoding circuits. The reliability, power, and complexity factors become considerably more important if higher basebands are necessary. For instance, for the 500-kc video spectrum now under consideration, the baseband

frequency for the orthogonal system becomes 8 mc with an RF bandwidth of 16 mc. The pulse counters, adders, etc. will become very complex for an 8-mc pulse rate. Thus, the PCM systems inhibit the growth of the VOIS package toward higher resolution capabilities.

A further advantage of FMFB accrues from the frequency characteristics of the electrostatic tape. It is found that, for a given black-and-white level, the percent modulation of the tape decreases with frequency (scanning rate), which would have the effect of reducing the equivalent modulation index of the transmitter. Therefore, for the same transmitter powers considered, pre-emphasis could be added to the transmitter to reduce the effect of noise on the high-frequency components of the intelligence. Pulse code modulation can not take advantage of this phenomenon of noise reduction. As a result, pre-emphasis will reduce the 4.3-db power advantage of orthogonal code systems over FMFB. It has been roughly calculated that sufficient pre-emphasis to maintain the required modulation index (see Section III.A.3) will reduce the carrier power by about 1.7 db. If an additional 1-db loss is included for a sampling rate slightly higher than ideal (as would be necessary in a practical case), and allowing 1 db for slicer imperfection, etc, then the difference between orthogonal coding and FMFB is only 0.6 db, assuming the most optimum numbers for the digital case. Considering all these factors, there are definite advantages to an FM system, especially for higher transmission rates (basebands).

The incorporation of either frequency compression or phase lock receivers into the DSIF can be accomplished by using a double heterodyne system in which the intermediate frequency of the DSIF receiver drives a separate super-heterodyne receiver of the frequency-compression or phase-lock type, which are specifically identified with the VOIS project. A simplified block diagram of this system is shown in Figure III-4.

3. Transmitter Power

It has been pointed out that the process of optimization will involve a progressive trade-off among camera equipment, transmitter equipment, and primary power. Assuming a set of system parameters, the transmitter size, weight, and primary power requirements can be calculated or estimated as an initial step in the optimization procedure. Subsequent evaluation of the VOIS package will reveal whether or not the choice was realistic. Changes in the DSIF will also affect these estimations.

The following assumptions will be made:

(a) Receiver improvement threshold = 6 db

(b) Output signal-to-noise ratio = 24 db (rms to rms). This ratio will result in a high-quality picture. An evaluation

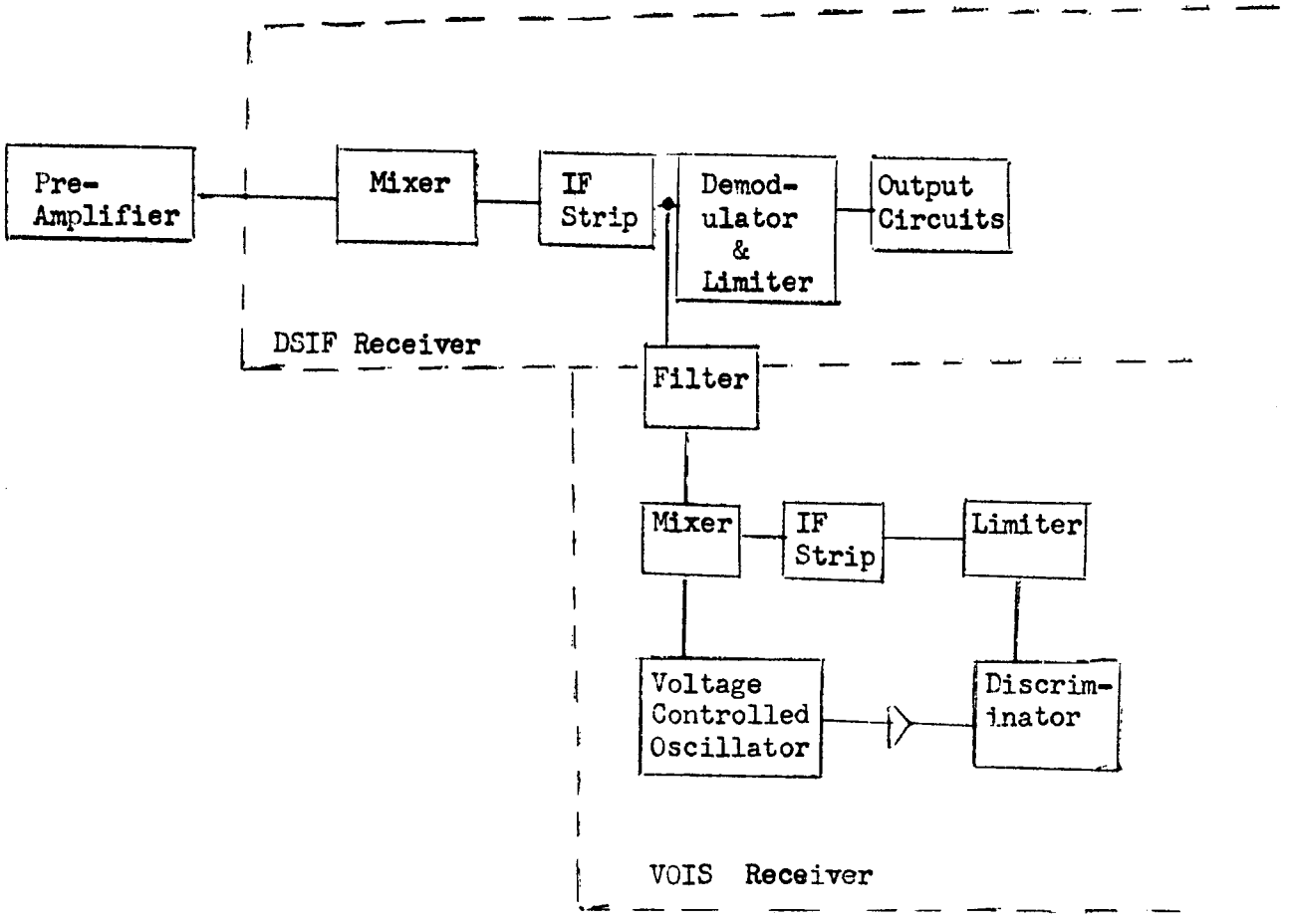

Figure III-4. Simplified Block Diagram of DSIF Receiver Modified by VOIS Requirements

of such pictures on the RCA TV simulator will reveal whether or not this ratio is a good choice for the lunar mapping mission.

(c) Baseband = 576 kc. This value is chosen in order to utilize the IF bandwidth of 4 mc. Uniform energy distribution in the baseband is assumed.

(d) RF bandwidth = 4 mc at 2300 mc.

(e) Modulation index = 2.5 (optimum value at a 6-db threshold).

(f) System noise temperature = 400°K. This assumes a 100°K receiver noise temperature, 250°K lunar noise temperature, and 50°K for atmospheric noise and sky noise. Sky noise, galactic noise, and solar noise are accounted for in the over-all system temperature. It may be desirable to investigate the possibility of other localized sources of sky noise for the particular DSIF sites selected. However, it is believed that this contribution to the system noise temperature is negligibly small. This system temperature is believed to be realistic and conservative because some safety factor is achieved in the large area of antenna illumination at 386,000 km.

(g) Free-space attenuation = 211.4 db.

(h) Ground antenna gain = 50 db.

(i) Satellite antenna gain = 26 db.

(j) System margins = 9 db, consisting of the following:

(1) Antenna pointing allowance = 2 db. (This assumes that optical sighting of moon will be used).

(2) RF losses (satellite) = 2 db. (Assumes a diplexer and a pre-selector filter).

(3) Polarization losses = 0 db.

(4) System deterioration = 5 db. (Accounts for RF misalignments, changes in power supply voltage, aging, etc.).

(5) Atmospheric (water, oxygen, precipitation) losses = 0 db.

With the above assumptions, the required transmitter power is 25 watts. A plot of transmitter power versus baseband frequency for various parameters is shown in Figure III-5. Note that power is directly proportional to baseband.

4. Transmitter Package

It is constructive to consider the general characteristics of S-band transmitters for the power levels we are currently considering. Table III-1 shows typical weights, efficiencies, and sizes for two different types of transmitting tubes, one using a negative grid (triode or tetrode) and the other using a traveling-wave tube (TWT) or klystron.

For power levels of less than 40 watts, state-of-the-art triodes, tetrodes, traveling-wave tubes, and klystrons are available, as well as voltage-tuned magnetrons for direct modulation.

The table is computed on the basis of over-all efficiency; that is, the screen and filament power are included in the estimate for the tetrode, and the TWT estimate includes helix and filament power, etc. The tetrode amplifier efficiency is higher for higher output powers, and this is reflected in the 25-watt transmitter. The higher efficiency, however, will increase the drive requirements and hence increase the modulator complexity. Higher-efficiency (output watts/pound) power supplies, (dc-to-dc converters) have been built by RCA for TIROS I; however, it seems realistic to reduce these efficiencies to account for the increased complexity involved with the higher voltages required.

The 2C39 class of planar triodes is a good example of a negative-grid tube for output power requirements of less than 20 watts. Suitable tetrodes are the RCA 6816 (15 watts at 2300 mc) and the GE Z5367 (40 watts at 3000 mc). Available TWT's are the RCA-A-1093 (15 watts) and the RCA-A-1166 (10 watts). Other examples could be cited; however, the important point is that numerous adequate power sources are available for these power levels, although some work may have to be done to improve reliability. The tetrodes and triodes are especially attractive with regard to long life, ruggedness, reliability, simplicity of associated circuitry, weight, and space.

It is believed that a transmitter power of over 100 watts is not a practical level for this experiment because of the primary-power and weight limitations; however, we will investigate the feasibility of achieving these higher powers if the system optimization procedure warrants it.

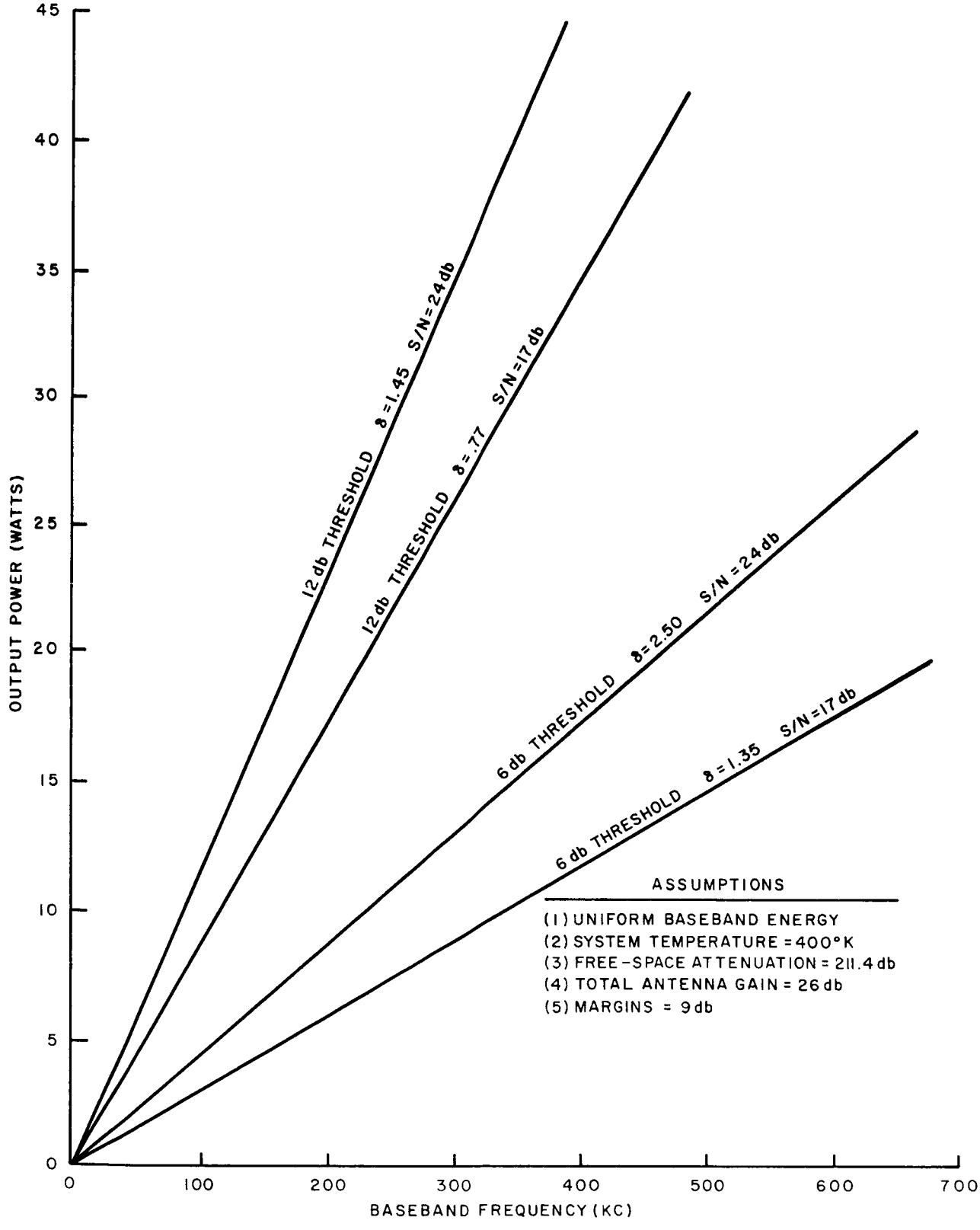

Figure III-5. Transmitter Power Output Versus Baseband Frequency for Various Parameters

TABLE III-1

Comparison of Estimated Transmitter Weight, Size, and Power Consumption for Negative-Grid and TWT for Two Values of Useful RF Output Power

11-Watt Transmitter	Triode or Tetrode Transmitter	TWT Transmitter
Tube Weight (lb)	0.25	7
Cavity Weight (lb)	2.0	-
Power-Supply Weight (lb)	14.0	14
Modulator Weight (lb)	7.0	5
Structure Weight (lb)	3.0	6
Total Weight (lb)	26.25	32
Power-Supply Output (watts)	142	142
Power-Supply Input (90% eff.) (watts)	158	158
Tube Dimensions (in.)	2x1-3/4	19x2

25-Watt Transmitter	Triode or Tetrode Transmitter	TWT Transmitter
Tube Weight (lb)	0.25	7
Cavity Weight (lb)	3.0	-
Power-Supply Weight (lb)	14.0	20
Modulator Weight (lb)	8.0	5
Structure Weight (lb)	3.0	6
Total Weight (lb)	28.0	38
Power-Supply Output (watts)	145	200
Power-Supply Input (watts) (90% eff.)	161	222
Tube Dimensions (in.)	3x1-3/4	19x2

5. Ground Command System

For relaying command signals from the earth to the vehicle, the following system has been assumed:

(a)	Ground Transmitter	10 kw = + 40 db
(b)	Transmitter Frequency	2100 mc
(c)	Ground Antenna Gain	50 db
(d)	Satellite Antenna Gain	26 db
(e)	Receiver Noise Bandwidth	2 mc
(f)	System Noise Temperature	4590°K
	(1) Receivers (crystal input)	NF = 10 db
	(2) RF plumbing loss	2 db
	(3) Receiver noise temperature	4300°K
	(4) Earth noise temperature	290°K
(g)	Noise Power	-129 dbw
(h)	Signal Power	-95.4 dbw
(i)	Margin	9 db
(j)	Signal-to-Noise Ratio	24.6 db
(k)	Doppler Shift	negligible in 2-mc bandwidth

It is expected that the command signals will utilize less than 1 kilocycle of bandwidth. However, since the transmitter power is available, it seems desirable to use it in order to simplify the satellite command receiver in the interest of reliability. The receiver would consist of a crystal-mixer input with a stable, but uncontrolled (no AFC), local oscillator. The local-oscillator drift necessitates the large bandwidth. The weight of the receiver, including the local oscillator and RF plumbing (preselector, mixer, diplexer), should be less than 2 pounds and require less than 10 watts of input power.

6. Environment

Launch and orbiting environments, as defined by "Spacecraft Environmental Specifications Flight Equipment, Ranger A1 and A2 Assemblies", have been examined. With the exception of exposure to Van Allen radiation, cosmic rays, etc. and the sterilization requirements, the environment is similar to that for present missiles and launching vehicles, for which transmitter equipment and associated electronics is "state of the art".

During the next period, the following system functions will be studied in more detail:

(a) Electrical characteristics of vidicon and electrostatic tape.

(b) Pre-emphasis as a means to improve picture quality (reduce noise).

(c) Special transmitter and modulator design problems associated with VOIS package.

(d) Parametric design of communication system and VOIS package.

B. ELECTROSTATIC STORAGE TAPE CAMERA

1. Basic Principles of Operation

a. The Storage Vidicon

In the normal vidicon, the photoconductor - by virtue of its associated capacitance - performs a short-time storage function in addition to its role as a photon detector. In the storage vidicon, the two functions are separated, and long-term storage is accomplished by the addition of an insulating layer to the target.

The electron-gun and target configuration for a typical storage vidicon are shown in Figure III-6. An equivalent circuit for the storage vidicon is given in Figure III-7. Here each target element - corresponding to a picture element - is represented by the insulator capacitance per element in series with the parallel combination of the photoconductor capacitance and resistance per element. The equivalent circuit element of the electron beam is the multiple-contact switch.

A simplified circuit can be used to describe the operation of the storage vidicon. Figure III-8 depicts a single target element, taking into account the relative orders of magnitude of the circuit resistors. The storage-vidicon operating procedure consists essentially of three steps: prepare, write, and read.

(1) Prepare - The signal plate potential is set at V_o, and the collector mesh at $V_o + V_1$. Referring to Figure III-8, $V_M - V_T = V_1$. The target is then exposed to a high-velocity beam, which drives the beam side of the target to collector potential. After a time greater than several circuit time-constants - from Figure III-8, $\tau = R_p (C_I + C_p)$ - a uniform potential difference V_1 exists across the insulator, independent of its previous charge distribution. The beam is then turned off. Typically, $V_o = 250$ volts and $V_1 = 25$ volts.

(2) Write - The collector mesh voltage is decreased to $V_o - V_2$, and the signal plate potential is left unchanged at V_o. Referring again to Figure III-8, $V_M - V_T = -V_2$. The photoconductor is then exposed to the optical image; simultaneously, the insulator is contacted by the electron beam, which causes the initial voltages across the insulator and photoconductor to decay. The discharge of the insulator is more rapid in areas where there is light on the photoconductor than where there is not. At some time T, the difference between the elemental insulator voltages corresponding to the light and dark areas of the photoconductor

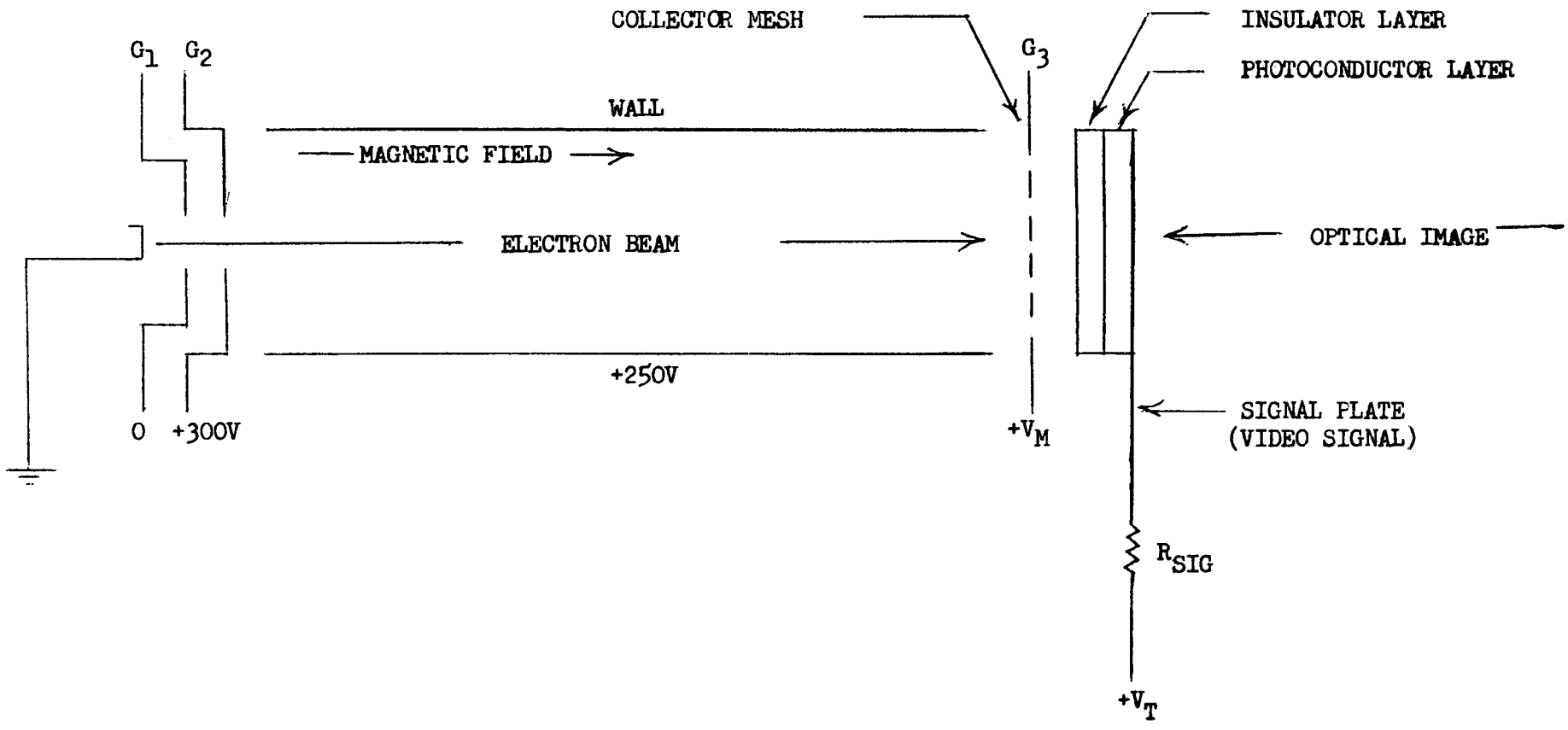

Figure III-6. Electron-Gun and Target Configurations for a Typical Storage Vidicon

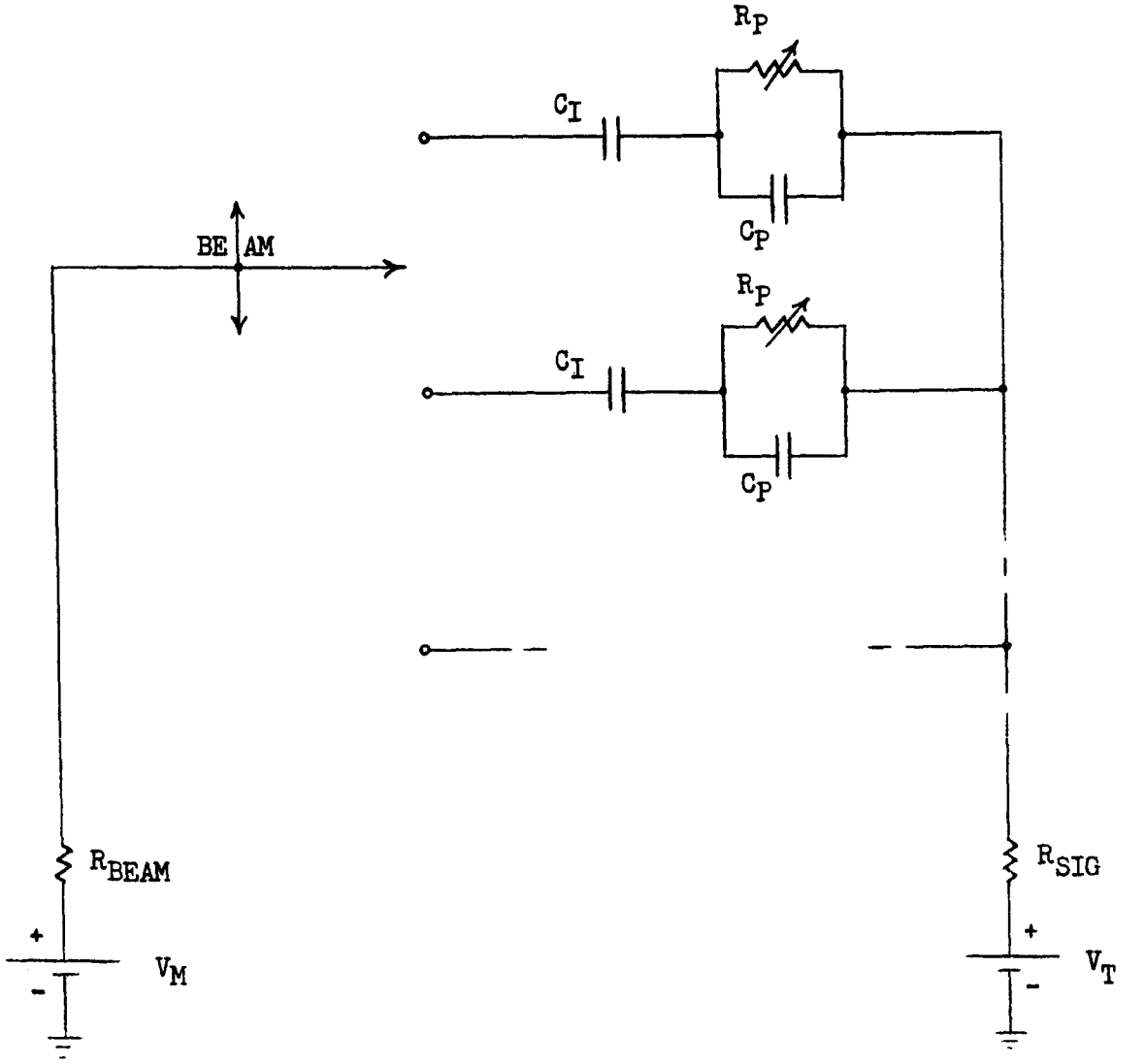

R_{BEAM} = Effective Beam Resistance

R_{SIG} = External Signal Plate Resistor

R_P = Photoconductor Resistance per Target Element

C_P = Photoconductor Capacitance per Target Element

C_I = Insulator Capacitance per Target Element

Figure III-7. Equivalent Circuit of Storage Vidicon

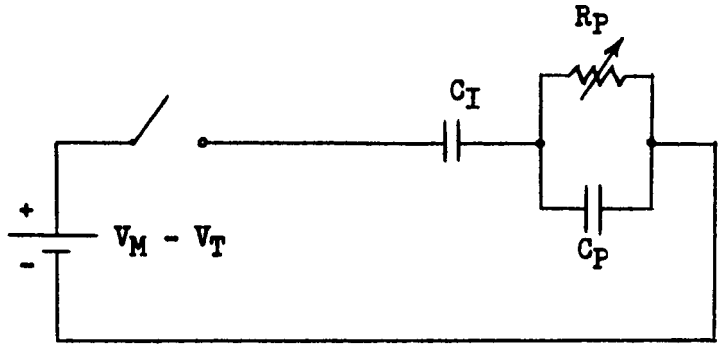

Figure III-8. Simplified Equivalent Circuit of Storage Vidicon: Single Target Element

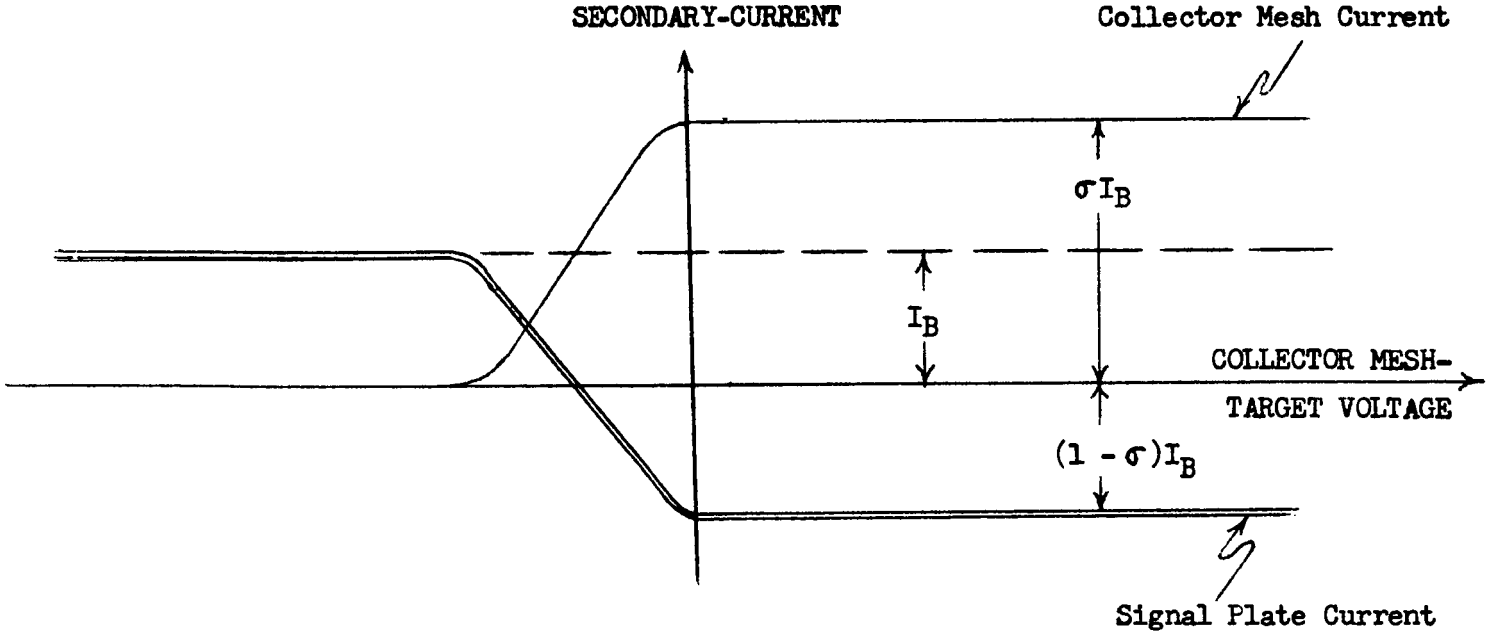

I_B = Primary Beam Current

σ = Average Secondary-Emission Ratio of Insulator

Figure III-9. Approximate Secondary-Electron Collector Characteristic of Storage Vidicon

is sufficient to produce, later in the read step, a good video signal. The electron beam is turned off at time T, and writing is terminated. The charge pattern on the insulator at time T is stored by its elemental capacitors; the only discharge paths are through the internal resistances of the insulators - not depicted in the equivalent circuits because of their extremely high value. Typically, V_2 = 25 volts.

(3) Read - The collector mesh is returned to V_o, the signal plate potential. Thus, in Figure III-8, $V_M - V_T = O$ and the elemental insulator and photoconductor are placed in parallel. The target area is scanned by the electron beam, and a video signal appears across the external signal plate resistor. Figure III-9 depicts the approximate secondary-electron collector characteristic of a storage vidicon, based on actual plots of collector mesh and signal plate currents as functions of the collector mesh-target voltage. As indicated in the figure, the signal plate current is proportional, within a limited range, to the difference between the equilibrium (collector mesh) and target surface potentials. The storage vidicon is operated within this range of current linearity. Therefore, when the target area is scanned by the electron beam, the resulting current variations in the signal plate are proportional to the charge distribution on the insulator. From Figure III-8, it is seen that, when the element scan time is much less than the circuit time constant, the insulator cannot be completely discharged. For this reason, the reading process is only partially destructive, and degradation in picture quality during successive readouts can be small.

Obviously, the procedure described above is only one of many methods available for operating the storage vidicon. The principles involved, however, will apply to any changes in the prepare, write, and/or read steps necessitated by system requirements.

Once the conditions for storage-target operation have been specified, it becomes necessary to determine an optimum target geometry for the storage vidicon. The problem becomes one of determining the insulator-photoconductor-layer capacitance ratio that will result in a maximum readout signal.

The analysis is straightforward if the storage-target photoconductor elements are assumed to act electrically like simple, linear resistors in parallel with elemental capacitors. A qualitative investigation shows that the stored signal increases as the layer capacitance ratio increases, and that the readout signal increases as this ratio decreases. The mathematical analysis results in a slightly greater than unity insulator-photoconductor-layer capacitance ratio.

b. Electrostatic Storage Tape

When pickup and storage of more than one optical image is required, the single-target storage vidicon becomes inadequate. For this reason, a camera device that can accommodate a great number of storage targets was devised. The combined optical pickup-electrostatic storage medium and flexible tape substrate is called electrostatic storage tape (EST).

The EST camera is essentially a multiple-target storage vidicon. A tape transport replaces the fixed-target assembly. Two electron guns may replace the single gun if separation of the write and read functions is desired. But, the same principles and techniques underlie the two devices.

EST construction consists of depositing, in the order named, a transparent conducting signal plate, a photoconducting layer, and an insulating layer on a flexible transparent base. The base presently used is Cronar, du Pont's movie-film base. The signal plate is a thin evaporated layer of gold, chromium, or other suitable metal. The photoconductor used for sensitivity in the visible red is antimony trisulfide, the chemical compound used in commercial vidicons. To date, the most successful insulating layer has been polystyrene. On each side of the sensitive area of the tape is a metal strip that serves as an electrical contact to the signal plate. The metal strips also act as spacers, preventing physical contact between adjacent layers of tape on the storage reels. A cross-sectional view of EST, indicating the thicknesses of the deposited layers of material, is given in Figure III-10.

2. Electrostatic Storage Tape Properties

With respect to EST, the properties of interest include storage time, resolution, sensitivity, spectral response, signal-to-noise ratio, gray-level response, and radiation resistance. Presented below are brief discussions of these topics. These comments will demonstrate the advantages and limitations of EST and indicate their effect on the VOIS design.

a. Storage Time

As part of its electrostatic storage program, the Radio Corporation of America has performed extensive research on organic and inorganic insulators for storage use. To date, the most promising storage layer has been polystyrene. This material can store electrostatic signals for several months and will withstand relatively high electric fields. Storage targets are easily fabricated by depositing polystyrene on the photoconductor from a glow discharge in styrene vapor. The many desirable properties of polystyrene make it a reasonable choice for EST.

The storage properties of EST have been demonstrated by the RCA Astro-Electronics Division in demountable and sealed-off cameras since 1958. Optical images have been stored on rolled-up EST for periods

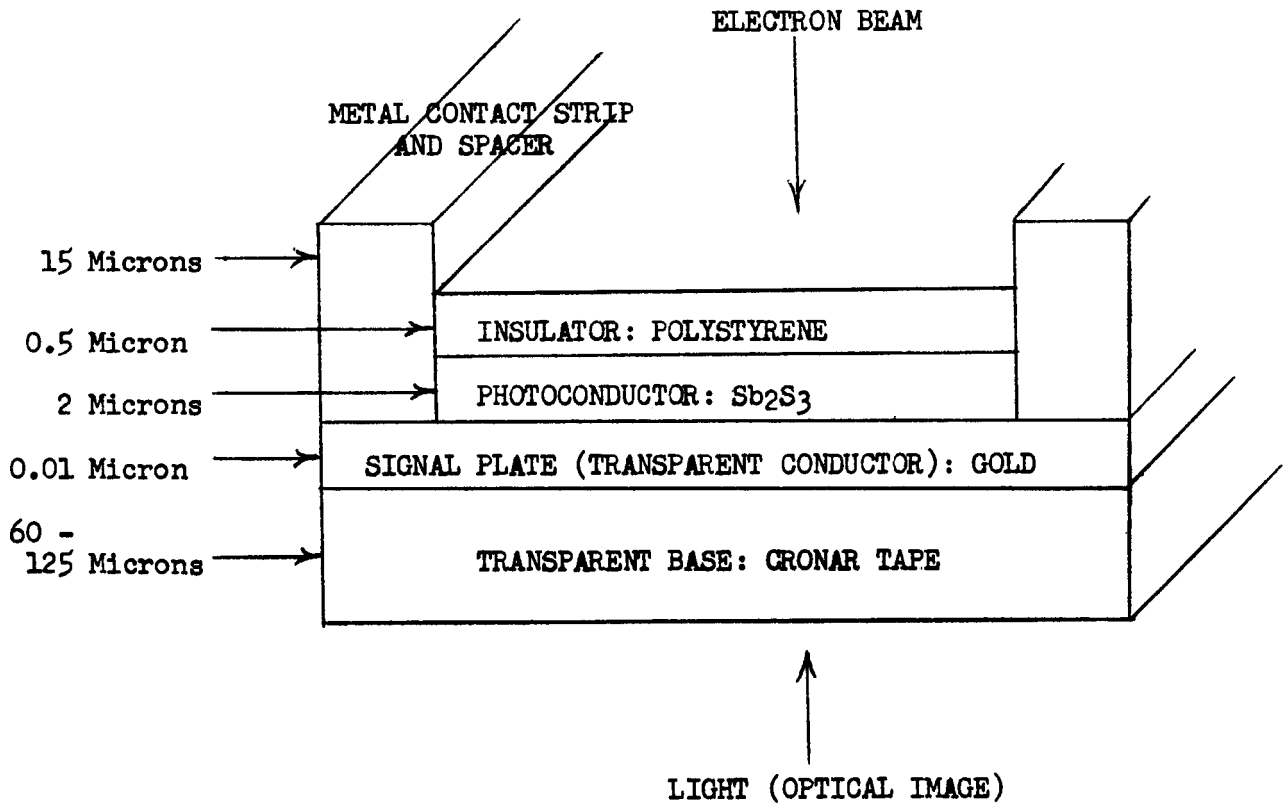

Figure III-10. Cross-Sectional View of Electrostatic Storage Tape

of 2 weeks and longer with no discernible deterioration of picture quality. Numerous photographs of pictures stored over various time periods are on file at the Astro-Electronics Division; they can be made available upon request.

b. Resolution

The limiting resolution of EST can be predicted from theoretical considerations. The three processes that affect the resolution capability are: light scattering in the photoconductor, photoelectron spreading in the photoconductor, and electrostatic field fringing across the insulator layer. The latter process has the greatest effect on tape resolution. Mathematical analysis results in an EST resolution limit exceeding 10,000 TV lines/cm, or 5000 optical line-pairs/cm.

The inherent tape resolution is sufficiently high so that it will not affect the over-all camera resolution. The latter will be determined solely by the resolution capability of the electron beam in the read process.

Both vidicon and image-orthicon readout techniques have been employed with storage targets. Production of a high-resolution beam is easier when the beam is made to approach the target at a relatively high velocity. As is the case with the standard image orthicon, high resolution is more difficult to attain if the beam approaches the target with an energy of 1 volt or less. The low-velocity beam spot is distorted by electric fields in the neighborhood of the target; the high velocity beam is not distorted.

High velocity return-beam readout is the technique to be employed by the VOIS camera. This readout technique has several advantages over the unmodified, high velocity vidicon mode. The gain in the electron multiplier results in an output signal of greater amplitude and a relaxed requirement on the beam-current magnitude. The latter, in turn, results in greater resolution. Since, in return-beam readout, the signal is taken from the multiplier and not from the backplate, the fact that long lengths of EST have large stray capacitances is of no concern. Finally, the secondary collector need not be a mesh, which fact should improve the over-all ruggedness of the camera and remove a possible limitation of the resolution.

The read-process electron beam will be focused via a long, axial magnetic field, which produces beam resolutions better than those obtained via electrostatic focusing. The fields are adjusted so that the transit time of an electron traveling from its source to the target, as determined by the internal electrostatic field, is equal to an integral number of periods about the magnetic field.

The read beam postulated for the VOIS camera is 0.01 micro-ampere, which is within the range of image-orthicon electron beam current.

Tests performed on standard image-orthicon guns at the RCA Laboratories produced a 0.01-microampere beam with 1900 TV lines/cm resolution. The measured sine wave response of a 0.01-microampere magnetically focused electron beam landing at the target with 50 volts is shown in Figure III-11. The limiting resolution, measured at 5% response, is seen to be 1900 TV lines/cm (950 optical line-pairs/cm). However, the resolution of the beam produced by a standard gun is sensitive to mismatch between the electrostatic and magnetic fields.

Although the problems of obtaining focus uniformity and stability are partially solved by providing excellent regulation and introducing dynamic focus correction, they are being approached directly at their source, the electron gun. Depth of focus has been improved by limiting the range of electron-velocity variation and adjusting entrance conditions for the beam into the magnetic field. Experiments on magnetically shielded, positive-grid guns have produced electron beams less sensitive, by an order of magnitude, to focus-electrode voltage variation than beams produced by standard image-orthicon guns. Present indications are that electron guns capable of producing 0.01-microampere, 2000-TV-lines/cm read beams will be state-of-the-art in less than 1 year. Experimental wide-deflection-angle, high-resolution guns are presently being built and tested by the Astro-Electronics Division and the RCA Laboratories. These guns are designed to accommodate EST of 70 mm width and greater. It is reasonably expected that these electron guns, which satisfy the requirements for the VOIS camera, will be in use before the 1962-63 period.

From the discussion of EST operation, it should be apparent that the prepare and write steps are best performed via an electron flood gun, rather than an electron beam gun. The flood gun must provide adequate current density, be rugged and simple, consume little power, and display no light output. The Schwartz gun, shown in cross-section in Figure III-12, most nearly fulfills these requirements. An experimental model of this gun produced a reasonably uniform 1.4-milliampere beam at the target. The total emission from the cathode was 3.9 milliamperes, which resulted in a 36% beam-forming efficiency. The total power input to the gun was 1.35 watts, of which 0.19 watt was used to heat the filament. The experimental unit was not ruggedised for use in satellites. An EST camera flood gun is being built for the Wright Air Development Division under Contract No. AF-33(616)-7284.

A more complete discussion of return-beam readout and electron guns will be given in the Final Report. Resolution, specified in this report by numbers of TV lines/cm, will be discussed more fully in the Final Report. An attempt to correlate photographic and television terms and parameters, with the objective of describing the capabilities of EST more satisfactorily, will also be made.

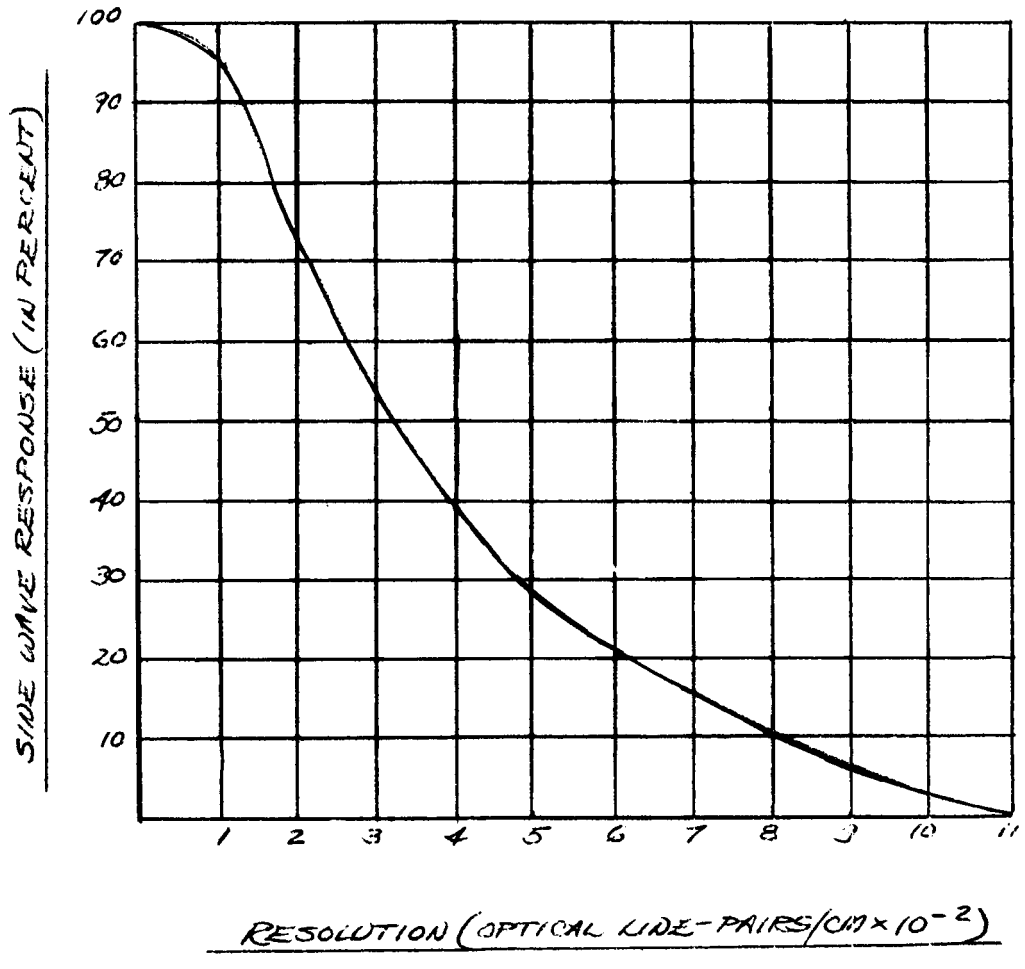

Figure III-11. Measured Sine Wave Response of a 0.01 μ α Beam

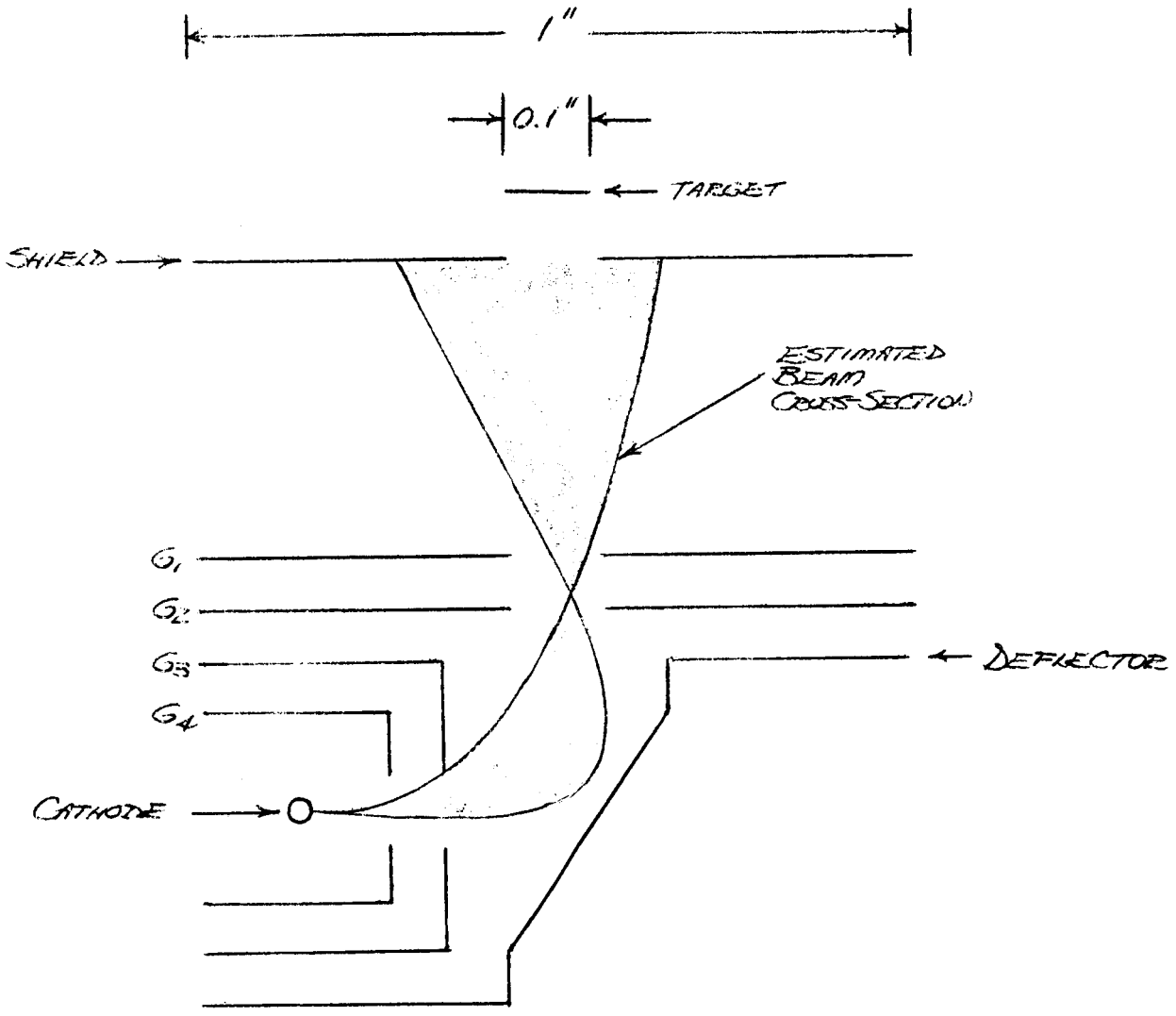

Figure III-12. Cross-Section of Rectangular Beam (Schwartz) Flood Gun

c. Sensitivity

Measurements have been made on EST which indicate that the photoconductor rise times are sufficiently fast for the reciprocity law to hold for exposure times of 1 second to 1 milliseconds. For exposure times in the range of the reciprocity law, the required EST photoconductor sensitivity can be estimated from the expression below.

$$S = \frac{C \Delta V}{E} \times 10^6,$$

where

S = required sensitivity in microamperes/lumen,

C = target capacity in farads/cm^2,

E = exposure in lumen-sec/cm^2, and

ΔV = peak-to-peak voltage swing on the target (above the black-level target voltage) or target signal in volts.

For a peak highlight exposure of 0.002 ft-candle-sec, $E = 2 \times 10^{-6}$. Using those values of parameters estimated to be 1962-63 state-of-the-art, the target signal is calculated to be $\Delta V = 0.75$ volts (which falls well within the range defining a linear portion of the secondary-electron collector characteristic) for $C = 2 \times 10^{-9}$ farad/cm^2. Thus, the photoconductor sensitivity must be 750 microamperes/lumen to meet the minimum exposure requirement.

Storage layers having photoconductor sensitivities exceeding 1000 microamperes/lumen are present state-of-the-art. Pictures obtained from 0.01 ft-candle-sec peak highlight exposures have been successfully imaged and stored on these targets. Present experiments indicate that 2000 microamperes/lumen, 0.002-ft-candle-sec EST will be available in the 1961-62 period.

Theoretical and experimental investigations of highly sensitive EST are being performed by the Astro-Electronics Division for the Wright Air Development Division under Contract No. AF-33(616)-6365.

d. Spectral Response

The spectral response of EST is determined entirely by the spectral response of the photoconductor. The spectral range of glassy antimony trisulfide, specified at the 50% of maximum points on the plot of quantum efficiency versus wavelength, extends from 0.5 to 0.7 micron.

Its maximum efficiency is about 0.54 and occurs at a wavelength of 0.6 micron (6000 Å).

Material can be added to antimony trisulfide to shift and/or narrow its spectral response as desired; for example, the response can be shifted to longer wavelengths. Other photoconductors are used to obtain required responses. Over 300 storage-targets, containing mixtures of many photoconductors, have been fabricated and tested. Many of these mixtures have been successfully deposited on EST. The spectral response curves for several materials (doped and undoped antimony trisulfide) are shown in Figure III-13.

Theoretical and experimental investigations of photoconductors, with emphasis on spectral response, are being performed by the Astro-Electronics Division for the Wright Air Development Division under Contract No. AF-33(616)-6365.

e. Signal-to-Noise Ratio

With respect to EST properties, it is important to consider the relationship between resolution and signal-to-noise ratio resulting from high-velocity return-beam readout. The basic information is contained in the secondary-electron collector characteristic. For an EST camera, the theoretical output signal-to-noise ratio is given by

$$\left(\frac{S}{N}\right)_o = \sqrt{\frac{p.n}{1 + \frac{2fC(\sigma + 1)}{kR^2}\left(\frac{I_oC}{kepnR^2} + 1\right)}} \quad ,$$

where

C = target capacitance in farads/cm^2,

e = electronic charge,

f = readout bandwidth in cycles/sec,

I_o = mesh secondary current returning from a black-level element on the target,

k = slope of linear portion of characteristic,

n = photons/TV bit in the optical image,

p = photoconductor average quantum efficiency,

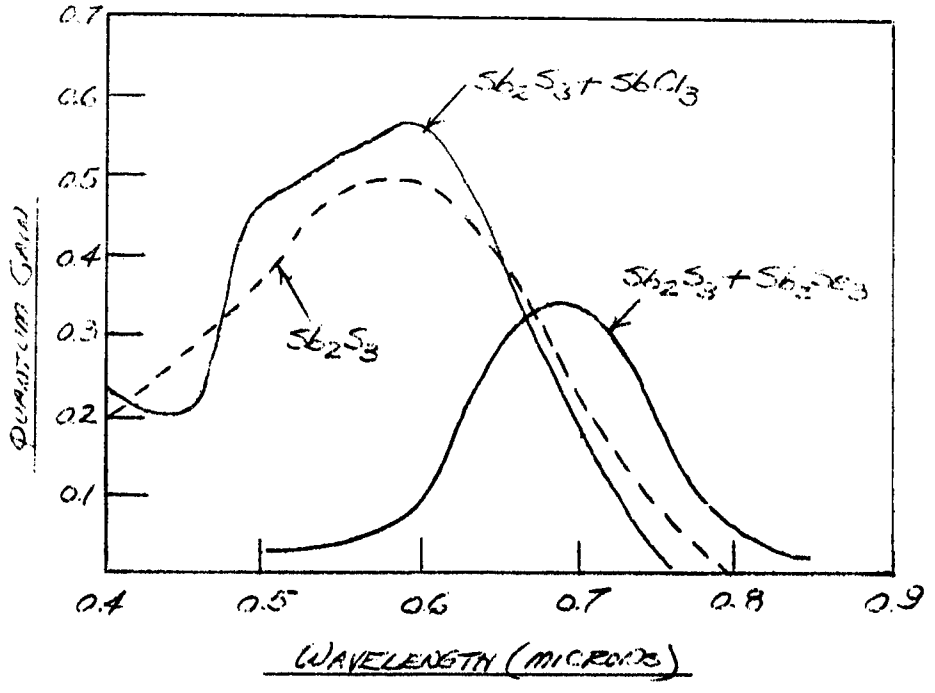

Figure III-13. Spectral Response Curves

R = TV lines/cm in the picture, and

σ = average secondary-emission ratio of insulator over the range of primary-electron energies from black to white level target voltage.

From experimentally determined secondary-electron collector characteristics (for polystyrene under 300-volt average primary-electron bombardment),

$k = I_B/10$,

$I_o = 0.5I_B$, and

$\sigma = 1.5$,

where I_B = primary beam current during readout.

Substituting the above values into the output signal-to-noise expression yields, for a photoconductor quantum efficiency of 1/3 electron/photon,

$$\left(\frac{S}{N}\right)_o = \sqrt{3 + \frac{150fC^n}{I_B R^2}\left(\frac{15C}{enR^2} + 1\right)}$$

For $C = 2 \times 10^{-9}$ farad/cm^2,

$e = 1.6 \times 10^{-19}$ coulomb/electron,

$f = 5 \times 10^5$ cycles/sec,

$I_B = 10^{-8}$ ampere,

Exposure = 0.002 ft-candle-sec

($n = 7 \times 10^3$ photons/TV bit) and

R = 2000 TV lines/cm,

($R^2 = 4 \times 10^6$ TV bits/cm^2),

$$\left(\frac{S}{N}\right)_o \approx 15 = 23\text{db}$$

These values pertain to the proposed VOIS operation and are based upon present estimations of the 1962-63 state-of-the-art.

For a good quality picture - one in which the background noise is barely visible - the minimum acceptable output signal-to-noise ratio is approximately 6 (15 db). The effects of resolution and output signal-to-noise ratio on picture quality are demonstrated by the television test patterns pictured in Figures III-14 through III-17. The four combinations of resolution and signal-to-noise ratio were realized via the TV simulator developed by the RCA Astro-Electronics Division for the purpose of picture evaluation.

f. Gray-Level Response

The number of gray levels which can be discerned in a picture readout from EST is determined mainly by the output signal-to-noise ratio and the sizes of the gray objects in the picture. The additive and subtractive nature of the noise or signal deviation at adjacent elements of the target determine the maximum and minimum limits of contrast reproduction. The maximum number of gray levels that could appear in the final picture is $L_{max} = (S/N)_o$, where $(S/N)_o$ is the output peak-signal-to-rms-noise ratio. The minimum number that would be contained in the output video signal is $L_{min} = (S/N')_o$, where $(S/N')_o$ is the output peak-signal/peak-to-peak noise ratio. For the background noise in a kinescope picture, the peak-to-peak value has been found experimentally to be about six times the rms value. Thus, $N' \approx 6N$ and $L_{min} \cong (S/6N)_o = \frac{1}{6}(S/N)_o = L_{max}/6$. The maximum and minimum conditions are the least likely to occur.

An analysis of the EST gray-level response would determine the effects of object size on the response from the statistics of the noise present in the picture. It has been shown experimentally that the response approaches L_{max} when the gray objects are large compared with a picture element; the response approaches L_{min} when the object size approaches that of a single element. If time permits, an analysis of the gray-level response will be attempted in the final period and presented in the Final Report.

In the previous section, the expressions and values given refer to the EST output peak-signal-to-rms-noise ratio. Thus, for the example cited, $L_{max} = 15$ and $L_{min} \cong 2.5$. EST contrast reproduction capability tests have been made with $\sqrt{2}$ density wedges; stored pictures of these wedges, when viewed with conventional display equipment, contained seven and eight gray steps.

g. Radiation Resistance

Theoretical considerations indicate that EST is not affected by high radiation. The amount of radiation absorbed by the storage layer

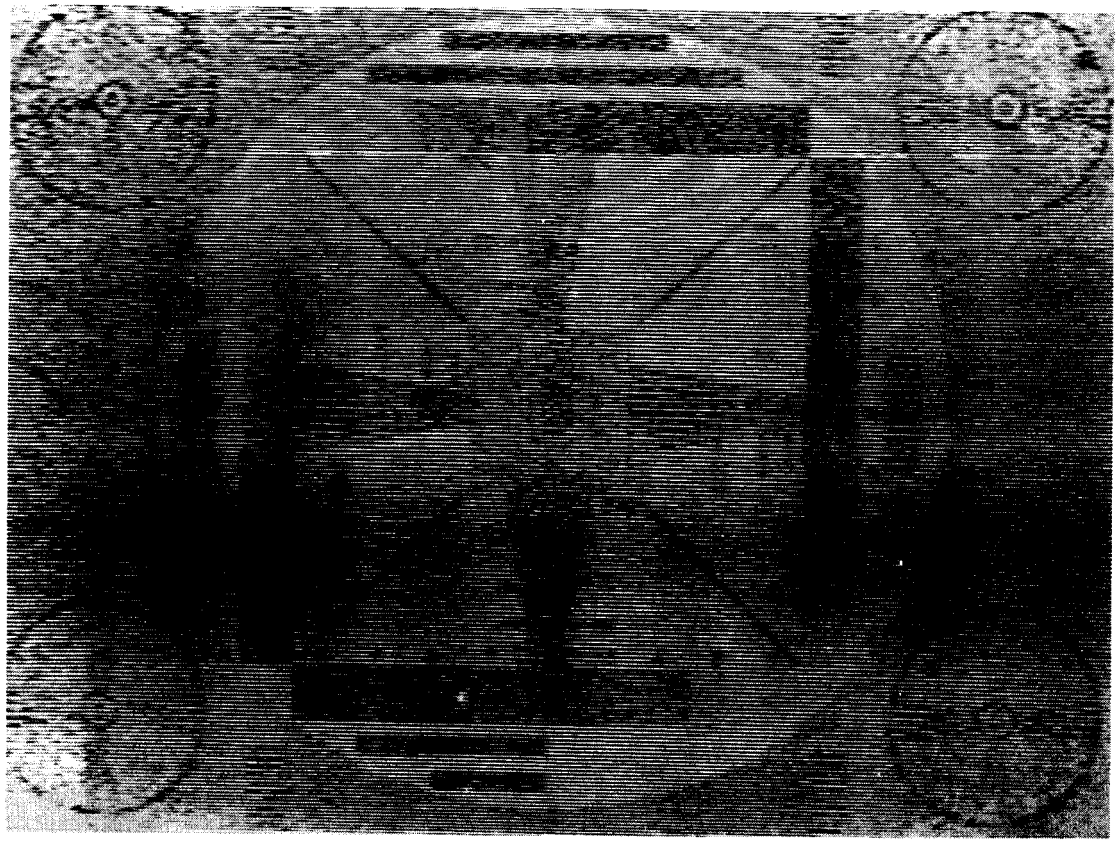

Figure III-14 250 Scanning Lines in Each Direction

3 : 1 (9 db) Signal-to-Noise Ratio

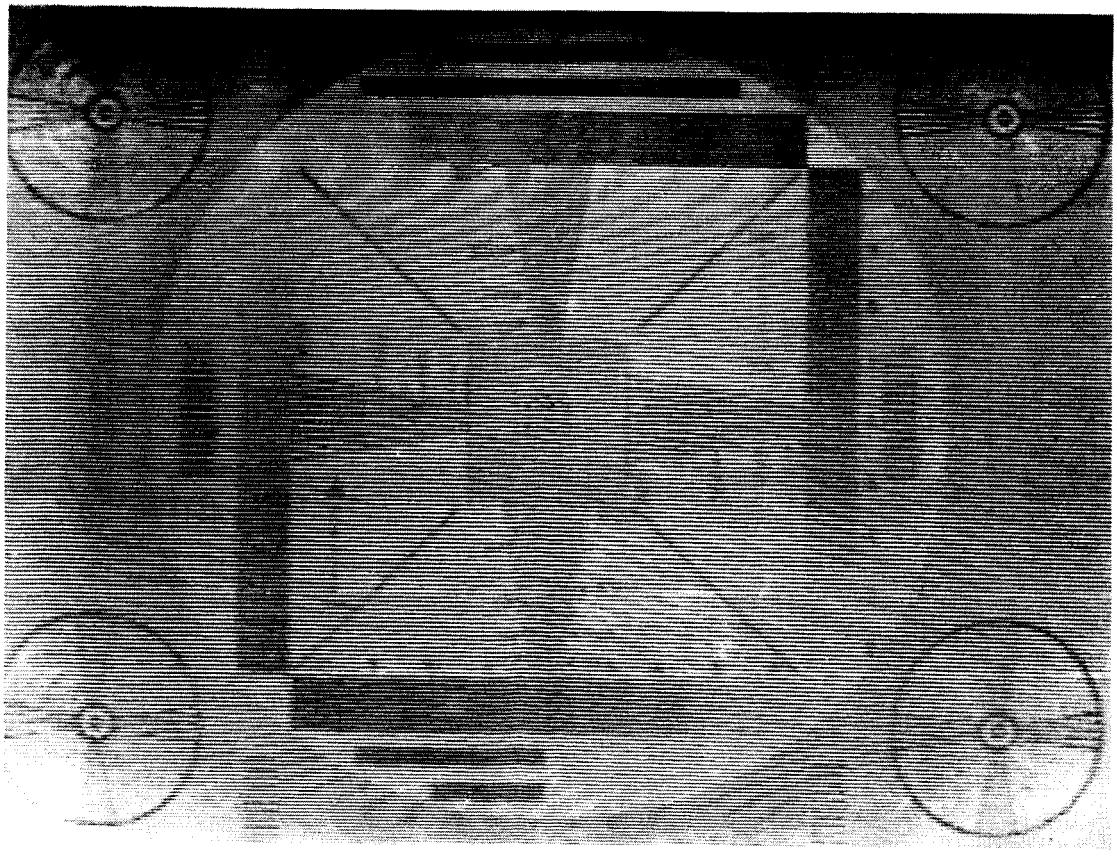

Figure III-15 250 Scanning Lines in Each Direction

10 : 1 (20 db) Signal-to-Noise Ratio

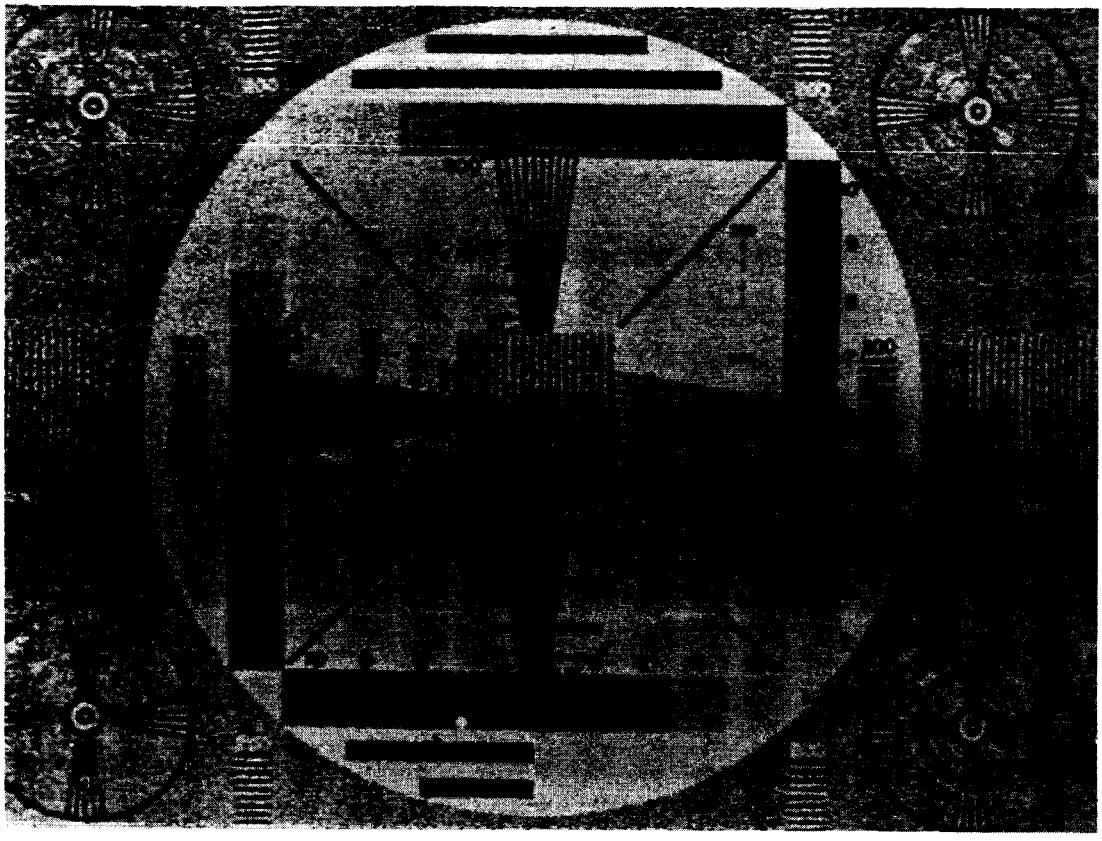

Figure III-16 500 Scanning Lines in Each Direction

3 : 1 (9 db) Signal-to-Noise Ratio

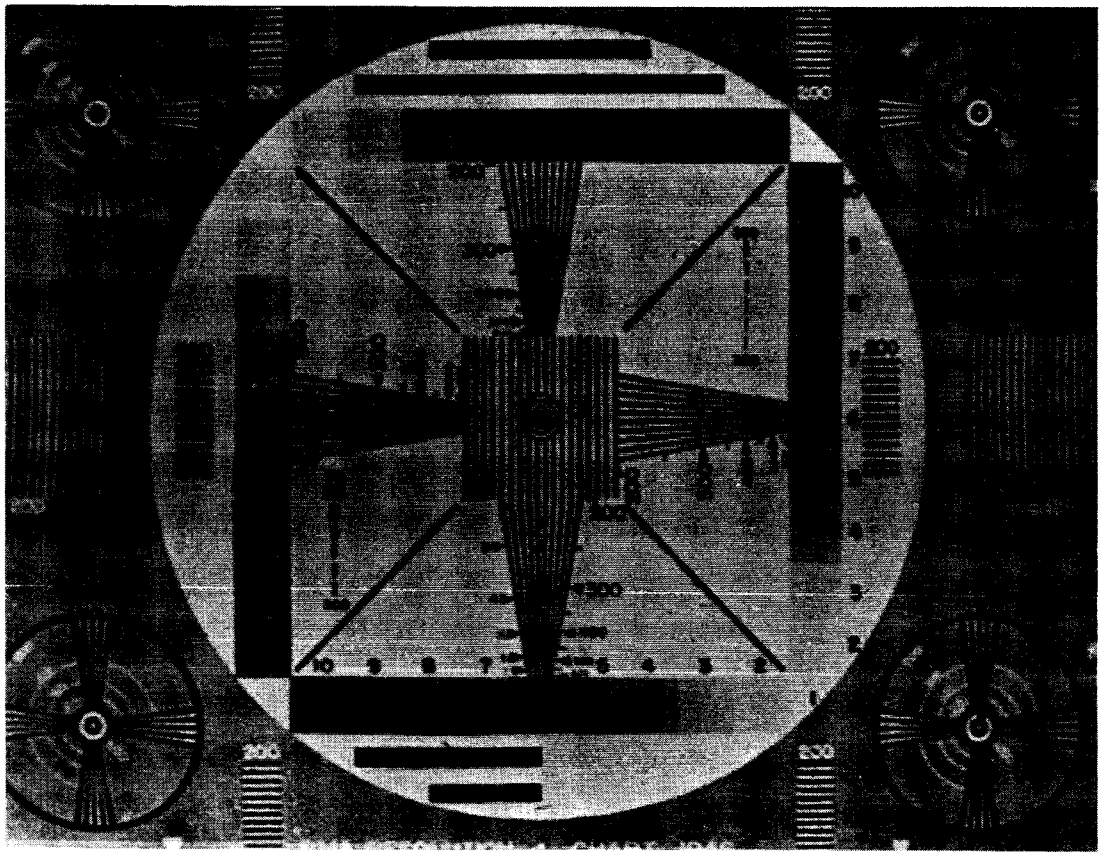

Figure III-17 500 Scanning Lines in Each Direction

10 : 1 (20 db) Signal-to-Noise Ratio

is only a small fraction of the incident radiation because of the low density and small thickness of the layer. As opposed to photographic film, EST is not sensitive to cumulative radiation; the target materials, however, will eventually decompose chemically.

A search of the literature shows that a vidicon with antimony trisulfide as the photoconductor was exposed to neutron and gamma radiation in the Brookhaven pile. No effect on the photoconductor was reported after sufficient exposure to darken the glass faceplate to 75% transmission. Reports also indicate that some types of polystyrene maintain adequately high resistivities under intense radiation, showing no color change even when exposed to 10^6 Roentgens of 2-Mev gamma radiation.

Experiments performed for the Astro-Electronics Division also indicate that EST is not affected by high radiation, bearing out the above presentations. A sample of glassy antimony trisulfide, the EST photoconductor, was exposed to 250 R/hr of 1-Mev X-rays in the RCA linear accelerator; no change in photoconductor conductivity was observed. Thus a radiation field of this intensity and energy would not appear as light to the photoconductor. A storage vidicon with an optical image stored on the target was exposed to 100 R/hr of 1-Mev X-rays for 1 hour. The stored picture, when read out some time later, appeared to be unaffected by the radiation.

3. Camera Design

Specification of the EST camera design is one of the more important requirements of the VOIS study program. At present, there are three major EST research and development programs being conducted at the Astro-Electronics Division. Research on EST and EST devices for satellite use is being performed for the Wright Air Development Division. An EST camera for meteorological satellite applications is being developed for the National Aeronautics and Space Administration. A research and development program for a high-resolution EST camera, similar to the VOIS camera, is also being sponsored by the Wright Air Development Division under Contract No. AF-33(616)-7284.

The discussions below should indicate the main areas of concern for the EST camera design. The proposed VOIS camera design will be presented in detail in the Final Report; estimates of the interface requirements are presented below. At present, the findings of the various EST programs are being studied and sifted for direct application in the VOIS camera design; these findings have already proved invaluable for this phase of the study.

a. Mechanical Design

The VOIS camera (excluding the optical system) will be

approximately 4 feet long, 2 feet deep, and 1 foot high. It will be rugged in design, permitting camera orientation in any direction. The complete camera, allowing 125 pounds for optics and 100 pounds for supporting structure, will weigh approximately 300 pounds. The addition of a second camera for three-dimensional plotting of the lunar surface will, of course, require an increase in the weight estimate.

For laboratory and pre-launch checkout of the VOIS, the camera enclosure will be required to maintain a vacuum of the order of 10^{-6} mm of mercury. The enclosure can be designed to accommodate a quick-disconnecting vacuum pump. A preferred method for obtaining vacuum, however, is via an electronic pump. At the Astro-Electronics Division, demonstration EST cameras and other enclosures have been successfully evacuated and maintained under vacuum solely by electronic pumps such as the Varian Vac-Ion Pump and the NRC Titanium Adsorber Pump. The electronic pump(s) for the enclosure would be small and light and would be mounted as a permanent member(s) of the VOIS camera structure; pumping action would be initiated by an external power source. Once the vehicle enters a high-vacuum environment, an enclosure diaphragm could be punctured to remove the residual pressure to the outer environment.

The main concern for the VOIS camera design is with the EST transport mechanism. A representation of the EST camera layout is given in Figure III-18. It indicates the design considerations required by the transport. The final design, to be presented in the Final Report, will be much more comprehensive than the layout indicates.

The VOIS camera will be capable of taking pictures of the lunar surface at high resolution and transmitting the stored information back to earth at high, medium, and low resolutions. With respect to tape speeds, this will require both continuous and stepped operation of the EST, the latter for high-resolution readout of small areas of the tape. The various speeds will also have to be adjustable within small ranges to adapt the camera to orbital variations and changes in altitude. For the same reasons, the time of exposure of the EST will also have to be variable within a small range.

With respect to vacuum techniques, an experimental (sealed) EST camera containing a length of tape, a stepping motor tape transport, and an image-orthicon gun was successfully operated by the Astro-Electronics Division. The parts used in the camera were made of standard materials specially selected for vacuum use. The tape transport was of nonmagnetic stainless steel. The mechanical parts received no processing for vacuum operation other than rigorous cleaning in toluene. The cathode emissive coating of thorium oxide provided for more than adequate gun emission and showed no signs of poisoning.

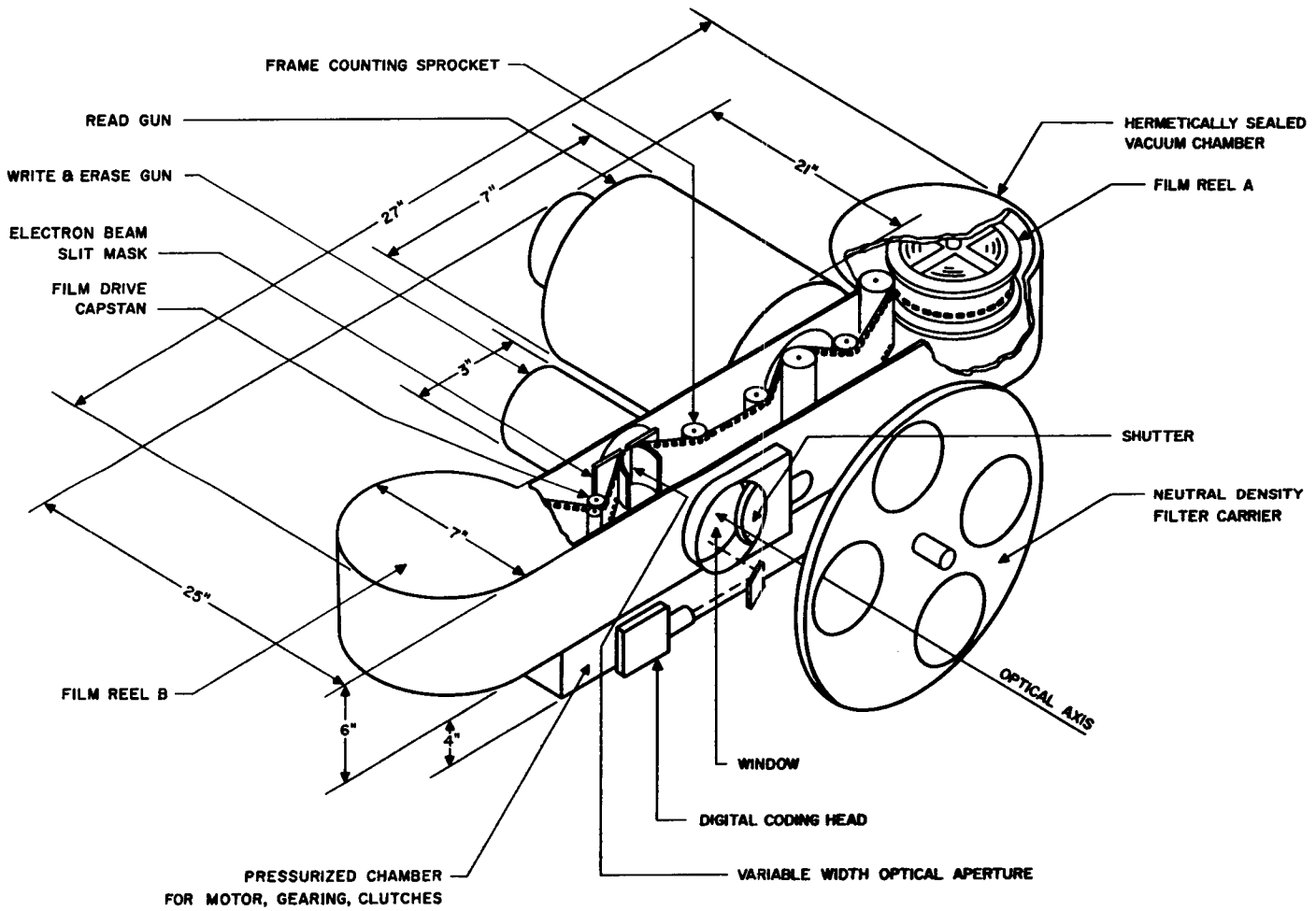

Figure III-18. Electrostatic Tape Camera Layout

The experimental tape transport mechanism used standard stainless-steel Barden ball bearings, which were carefully washed to remove all traces of lubricant. For devices like the VOIS camera, which require more tape motion and consequently more bearing wear, several types of bearing have been shown to be suitable. Bearings were tested and some are still under observation, in devices like the sealed tube of Figure III-19. Barden Bartemp retainers were found to provide dry lubrication; Barden bearings have run successfully for 10^8 revolutions. Machlett silver-lubricated bearings, similar to those used in rotary-anode X-ray tubes, were successfully tested in vacuum. Stellite bearings ran well in an oil-pumped system, but their high cost makes them less attractive than the other bearings.

The nature of EST and the high precision required of the transport parts make high-temperature vacuum baking of the camera elements undesirable. Bulk sterilization of the camera will be required. From experiments performed on these materials, it is necessary to specify the allowable temperature range of the tape and tape transport combination as 0 to 50°C. Vacuum techniques continue to be studied and developed at the Astro-Electronics Division. A comprehensive discussion of vacuum techniques and their direct application to the VOIS camera design will be given in the Final Report.

b. Electrical Design

As stated above, the VOIS camera will be required to transmit pictorial data to the ground at high, medium, and low resolutions. The three levels of resolution can be achieved by filtering the high-resolution readout signal or by defocusing the electron beam during readout. The latter method is preferred because it is simple, easy to enact, and eliminates the need for additional equipment.

Present thinking indicates that the camera design will incorporate a flood gun for erase and write operations, and several electron-beam guns for readout. One gun, which can scan a portion of a tape frame, will be devoted to high-resolution readout; the frame will be stepped into position as desired by ground signal to the transport programmer. Two guns will be defocused from the high-resolution condition to provide for medium-resolution slit readout of continuous moving tape (for mapping); further defocusing will produce the desired low-resolution pictures (for correlation). Further study will indicate whether any more guns will be required and/or desirable. The final design of the VOIS camera will incorporate the results of this investigation.

The basic circuitry required by the VOIS cameras will be very similar to that being developed by the Astro-Electronics Division for the Wright Air Development Division under Contract No. AF-33(616)-7284. High stability and linearity will be required of the circuitry to attain

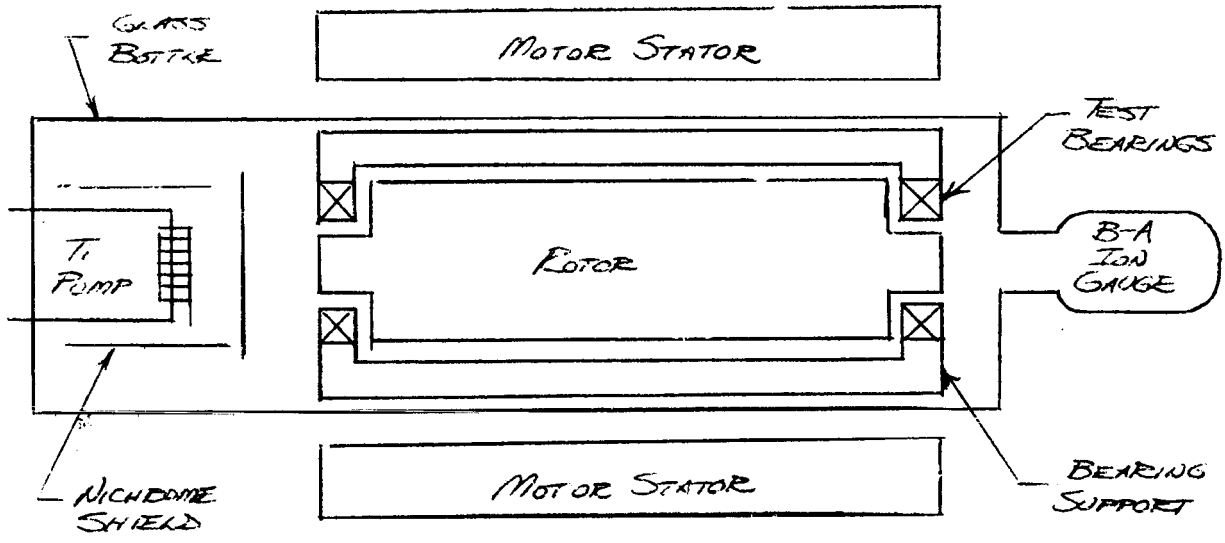

Figure III-19. Bearing Test Device

the high-resolution readout. The optimum scanning rates, which will be specified in the Final Report, must also conform to the high-resolution requirement. The basic circuitry will include video amplifiers, focus supplies, deflection generators, and sync and blanking generators. The specifications for this equipment will be given in the Final Report.

A programmer will be required to control the tape transport operation, which includes the tape frame positioning and the voltage switching required by the various erase, write, and read operations.

The VOIS camera and its associated circuitry are expected to require approximately 50 watts of power during normal operation.

4. Electrical Signal Recording

There is underway at the Astro-Electronics Division an RCA-supported study of electrostatic tape in general. Under the applied research program, applications other than the direct recording of optical data via EST are being investigated. The results of the effort to date indicate that electrical signal recording can be performed by electrostatic tape. The recording of analog and digital input signals has been successfully demonstrated. Because electrostatic tape has inherent and demonstrated advantages (e.g., higher packing densities, longer life and reusability, and higher radiation resistance) over magnetic tape for the storage of these data, the effort will be increased in 1961.

a. Analog Signal Storage

In the analog recorder, the storage medium consists of an insulator (e.g., polystyrene) layer deposited on a Cronar substrate. The photoconductor layer, required by EST for optical sensing, is omitted in the signal recorder. The electrical data to be stored are applied as input signals to the control grid (or cathode) of an electron-beam gun. Writing and reading can be performed via the same electron gun in the signal recorder.

With respect to electrostatic tape properties, it is important to consider the relationship between data packing density and signal-to-noise ratio resulting from high-velocity return-beam readout. For an analog signal recorder, the theoretical output signal-to-noise ratio is given by

$$\left(\frac{S}{N}\right)_o = \sqrt{\left[1+\frac{1}{\frac{2fC(\sigma+1)}{kR^2}\left(\frac{2fCI_o}{kI_BR^2}+1\right)}\right]\frac{I_B}{2ef}},$$

where R^2 is the data packing density in bits/cm^2, and the other parameters are as defined in Section III. B. 2. e.

Substituting the experimentally determined values of k, I_o, and σ into the output signal-to-noise expression,

$$\left(\frac{S}{N}\right)_o = \sqrt{\left[\frac{1}{1+\frac{50\,fC}{I_B R^2}\left(\frac{10fC}{I_B R^2}+1\right)}\right]\frac{I_B}{2ef}}$$

An electron gun capable of resolving 2000 TV lines/cm can effect an analog signal recorder packing density of $(2000/\sqrt{2})^2 = 2 \times 10^6$ bits/cm^2, the $\sqrt{2}$ factor accounting for the cascade of the write and read apertures.

For $C = 10^{-9}$ farad/cm^2,

$e = 1.6 \times 10^{-19}$ coulomb/electron,

$f = 2 \times 10^6$ cycles/sec,

$I_B = 10^{-8}$ ampere, and

$R^2 = 2 \times 10^6$ bits/cm^2,

$(S/N)_o = 37$ (31 db).

These values are based upon present estimations of the 1962-63 state-of-the-art. For readout bandwidths of less than 2 megacycles, the recorder signal-to-noise ratio would exceed 37. The recorder typified by the above values would be capable of resolving better than 6 analog steps.

For the VOIS system, analog storage could be performed in a separate electrostatic tape recorder or in the EST camera itself. Recommendations based on further study of the possibilities will be made in the final report.

b. Digital Signal Storage

In the digital recorder, the storage target consists of a metal backplate (deposited on a suitable substrate) covered by a mosaic of bits of insulator material (e.g., polystyrene). The electron gun, which operates the tube in both the high-and low-velocity modes, has a sharply focused beam which can be positioned to a point on the target by applying appropriate voltages to the deflection yoke. Input signals for writing information onto the target are applied to the cathode and coupled control grid of the write-read gun as either positive or negative pulses. Data readout signals are

obtained from an electron multiplier. Charges lost by the individual storage bits can be replenished so that they are maintained indefinitely at the potentials established in writing.

An analysis of the operating procedures for a prototype binary electrostatic storage tube was performed by the Astro-Electronics Division. A relatively simple tube would incorporate standard 3-inch image-orthicon design and components, store 400,000 bits (at 250,000 bits/inch^2 packing density), and feature a 1-megacycle/sec data rate for writing. The required writing-beam current is approximately 0.75 microampere. The 400 TV lines/cm resolution required of the beam is achievable with standard image-orthicon guns. The theoretical readout signal-to-noise ratio expressions predict reading data rates of several megacycles/sec and greater. Feasibility tubes are being designed, fabricated, and tested for the RCA-sponsored applied research program.

Significant increases in data rates and packing densities are dependent upon the progress of the research programs for electron guns currently under way at the Astro-Electronics Division and the RCA Laboratories. For exceedingly high packing densities, the storage-target can be constructed to provide for closed-loop control of the electron-beam position on the target.

For the VOIS system, digital storage could be performed in a separate electrostatic tape recorder or in the EST camera, provided the tape in the camera is fabricated with the insulator mosaic in specified areas. Recommendations based on further study of the possibilities will be made in the final report.

C. OBJECTIVE LENS

Light-gathering and image-forming requirements establish the aperture and focal length for the optical objective lens. Because of weight limitations, the use of dioptric systems was excluded and a catadioptric system selected for the VOIS, since catadioptric systems can be made of lightweight materials. Dr. James G. Baker designed a catadioptric system for an aerial mapping camera which was built by the Perkin-Elmer Corporation. An optical schematic of this catadioptric system is shown in Figure III-20. The system consists of a positive corrector lens, a primary concave mirror, a Mangin secondary mirror, and a dioptric lens group. Some modifications of this basic system will be required to satisfy the electrostatic tape format size resulting in a reduction in angular field. Preliminary analysis indicates that a system with an equivalent focal length of 91.44 cm and with a relative aperture of f/2.5 might be obtained for a reasonable weight (approximately 100 pounds).

One of the disadvantages of catadioptric systems is the obscuration caused by the secondary mirror with a resultant loss of illumination. Figure III-21, derived by the Perkin-Elmer Corporation, gives the sinewave response for the basic Baker catadioptric system. To determine the transmission factor for a given level of resolution, consider the case of a periodic test object having a 1-meter period and imaged by the optical system from an altitude of 200 kilometers. The limiting resolution, v_o, is given by

$$v_o = \frac{1}{N\lambda},$$

where N = f/#, the relative aperture; and

λ = average wavelength = 6×10^{-4} mm.

The frequency, v, in the image plane is given by

$$v = \frac{h}{d\,f},$$

where h = object distance = 200 km,

d = period of the test object = 1 m, and

f = focal length of the objective lens.

For N = 2.5 and a focal length of 36 inches (91.44 cm), v_o = 667 cycles/mm and v = 243 cycles/mm. Computing the value for x (the abscissa of Figure III-21) we obtain

$$x = N\lambda\, v = \frac{v}{v_o} = 0.364$$

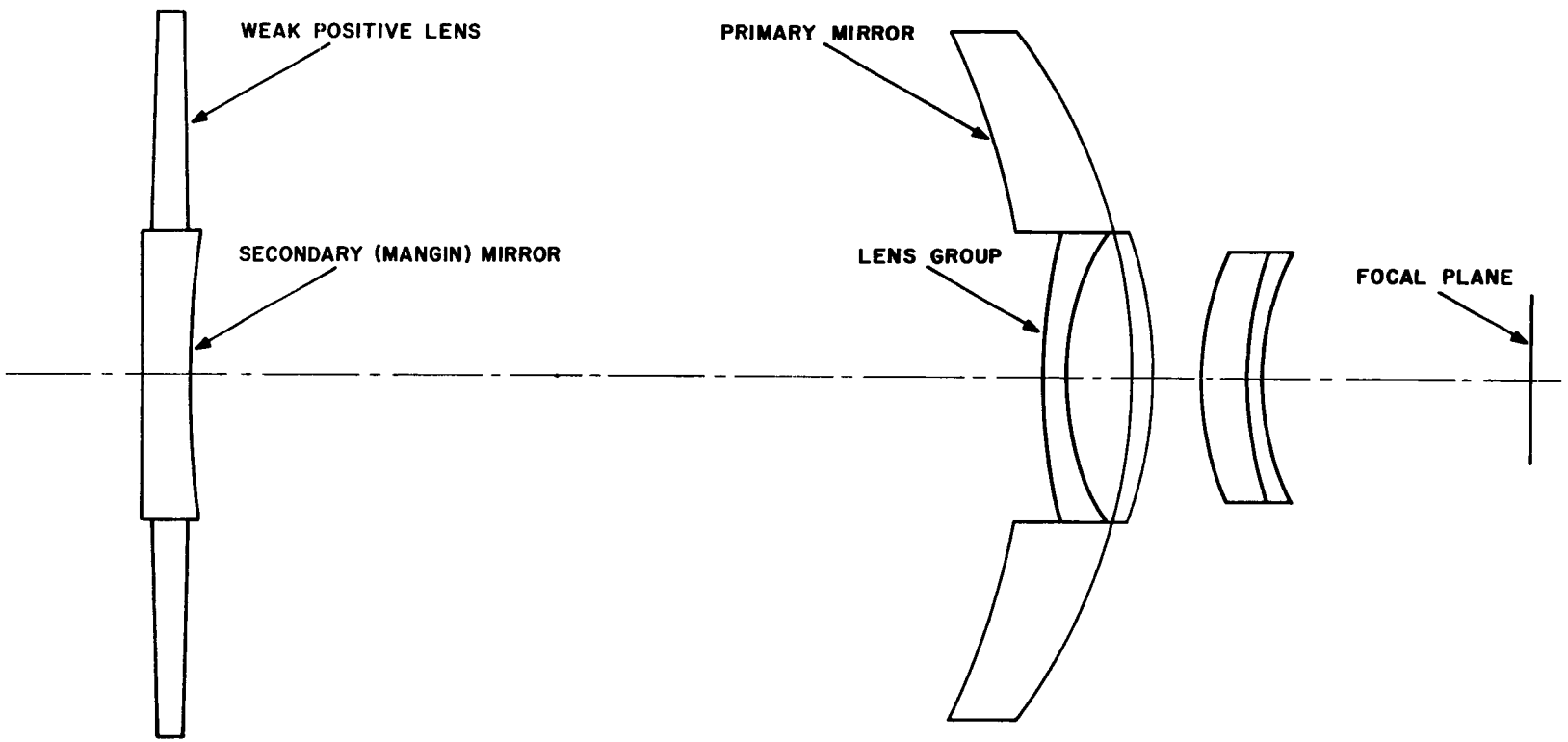

Figure III-20. Optical Schematic

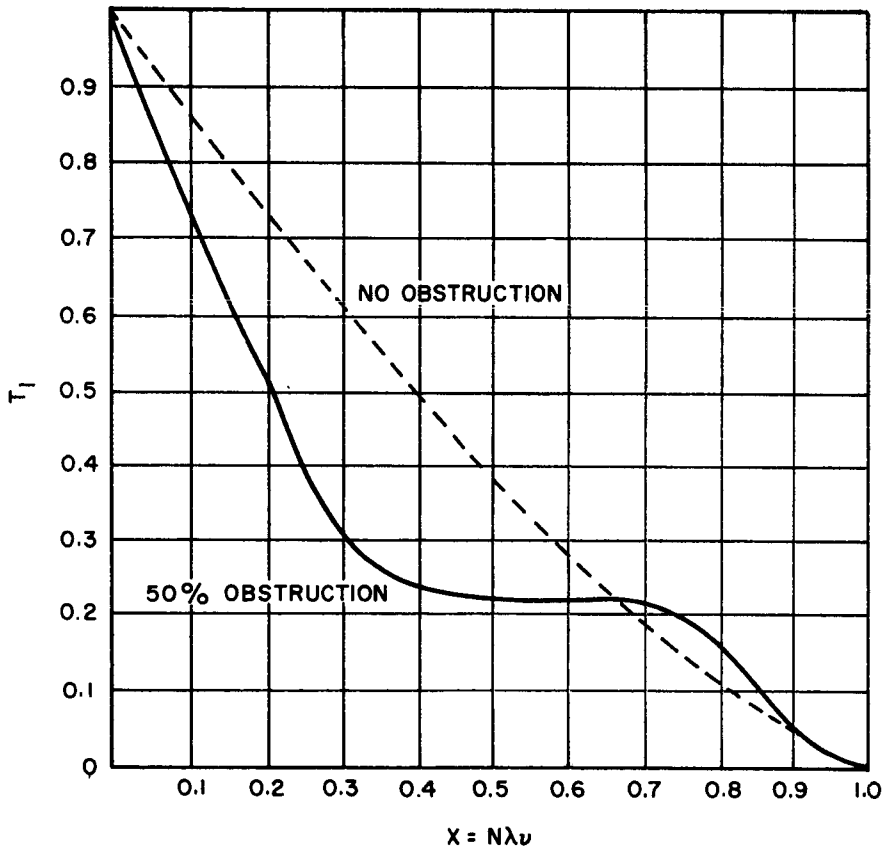

Figure III-21. Comparison of Theoretical Line-Wave Response of Obscured and Non-Obscured Optical Systems

Entering the figure for this value of x, the sine-wave response of the lens system is found to be 25% using the 50% obscuration curve.

The angular resolution of the optical system is 0.45 second of arc and is derived from the Rayleigh criterion as given by

$$\alpha = \frac{1.22\,\lambda}{d} ,$$

where α is the angular resolution,

λ is the wavelength, and

d is the aperture diameter.

The angular subtense of 1 meter at 200 kilometers is 1 second of arc, which is above the theoretical diffraction limit of the optical system. Table III-2 is a tentative list of the optical system parameters for the VOIS.

The optical-system alignment will require further detailed study. Some preliminary results can be given at the present time. Before launch, alignment of the corrector plate and the Mangin mirror can be accomplished and the system fastened to the main lens housing so as to withstand vibration and acceleration moments. The primary mirror and the lens group can be securely fastened to each other. It is anticipated that the primary-mirror cell assembly may have some rotational misalignment with respect to the main lens housing, caused by vibration and acceleration. To obtain maximum resolution output requires that the optical system maintain high accuracy in angular alignment. This may necessitate automatic adjustment of the primary cell after injection into orbit. Another contributing misalignment factor is thermal variations which may cause defocus of the system. Thermal effects on optical members in terms of defocus and misalignment will be studied in the next period.

To reduce the weight of the primary mirror, materials will be used that have light weight, low thermal coefficients, and good optical stability. Some of the materials that have been developed and are in the process of testing are foam quartz, fuzed quartz, fuzed silica, pyroceram, and glass castings. Weight savings of the order of 30% to 70% may be achieved with these materials.

The use of radiation-protected optical glass is limited to a very few types of glass. For example, Bausch & Lomb glass catalog lists three types of crown and two types of flint glasses. Even these glasses can only withstand low-energy and short-time dosages of radiation. In the Baker catadioptric system, the lenses may be recessed so that no direct radiation can reach them, thus providing a degree of radiation protection.

With regard to stereoscopic or contour mapping capabilities of the system, some stereoscopic representation may be possible with the low-resolution,

two-dimensional mapping system where the percentage of overlap from orbit to orbit is sufficiently high. If the system is capable of 10% overlap, at the lunar equator, then at latitudes greater than 30° the percentage of overlap will be greater than 50% and more than 100% for latitudes greater than 60°. The major problem here is one of registration after receiving the transmitted data on the earth, since the baseline between the two views is continually changing with latitude. During the next period of the study program, a detailed analysis will be made to determine the quantitative data which can be obtained from this stereoscopic presentation.

TABLE III-2

Optical System Parameters

Type of System - Modified Baker Catadioptric Objective

Focal Length - 91.44 cm

Relative Aperture - F/2.5

Image Size (For Slit Camera) - 6 cm x 1.37 x 10^{-3} cm

Sine-Wave Response over Full Field Angle - Not less than 30% at 200 lines/mm

Approximate Dimensions - 40 cm x 47 cm

D. STRUCTURE

The VOIS package, as presently conceived, contains a scanning mirror, a high-resolution optical system, a tape camera, associated electronic circuitry, and several servo-controlled drive units for orienting and adjusting the optical units and camera while in orbit. (See Figure III-22.)

The main structural problem concerning the VOIS package is that of designing a structure which will minimize the shear and tensile forces acting on the mirror and lens surfaces, since it is necessary that the alignment of the optical system be maintained to a high degree of accuracy. If the main structure is not sufficiently rigid, excessive stresses may be sustained by the mirrors and lenses, resulting in strained and wrinkled surfaces. This is more likely to occur during the launching and orbital injection phases. To prevent this condition, all mirrors and lenses have been arranged so that their (flat) surfaces will be in the plane of the thrust of the rocket and retro-rocket motors. This means that they will be in compression during the period of severe loading (see Figure III-23). Glass is at least four times stronger in compression as in tension and if properly supported will not fail in compression.

Vibrations will be a problem both during the launch and operational phases. To prevent excessive vibration and shattering of the large mirrors, stiff frame supports have been incorporated around the periphery of each unit. These frames are in turn supported by the main structure.

Isolation of the tape-camera reel drive units will not be a serious problem, but elimination of vibrations caused by the reciprocating motion of the scanning mirror will be difficult. Scanning rates require that the return motion of the mirror be about three times faster than the forward scan motion. This motion may be accomplished by the action of two cams superimposed on a follower arm, resulting in the reciprocating motion of a lever arm which drives the mirror through a pinion gear. Another method which would require fewer moving parts and would also constitute a positive drive would be an electromagnetic-solenoid-type mechanism. This system would utilize opposed drives and would provide natural damping for the system.

The scanning rates will depend upon the orbital velocity and the height above the moon, so provisions must be made to vary the scanning rate of the mirror, which would not be too difficult for either mechanism. This motion will not only set up vibrations but will also introduce unbalanced torques into the system. This method of driving the scan mirror will be given particular emphasis during the next period.

The major requirement for temperature control will be necessitated by the critical adjustments required in the camera and the optical systems. The

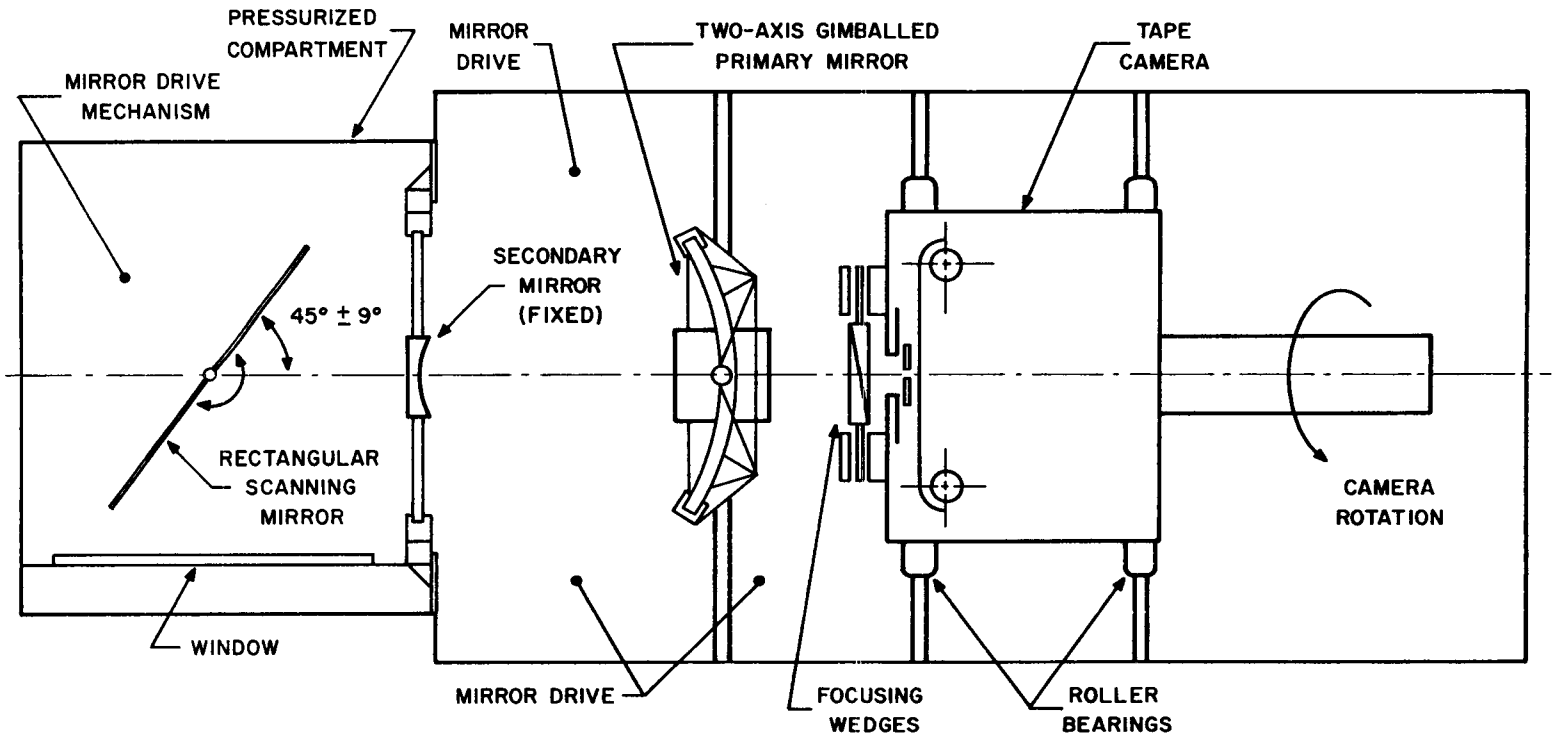

Figure III-22. Camera System Layout

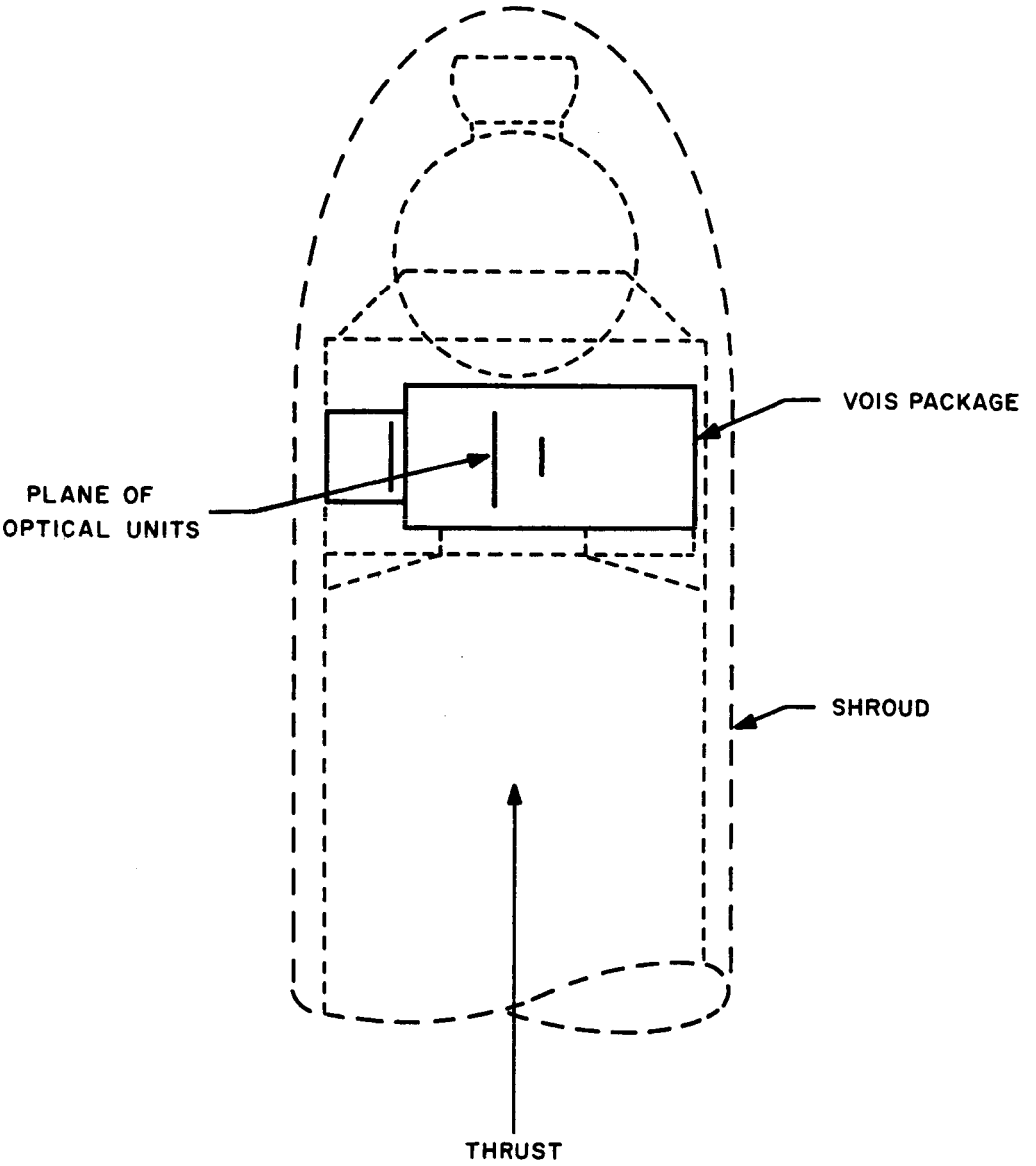

Figure III-23. Arrangement of VOIS Package During Launch and Orbital Injection Phases

specific problems concerning the structure are possible damage or distortion because of thermal expansion of the optical components and warping of the structure caused by thermal expansion with subsequent misalignment of the axis of the optical system. To obviate thermal stresses in the optical components caused by differential expansion, suitable structural materials having the same coefficient of expansion as glass are being investigated. It is expected that the main structure itself will be of light sheet-metal construction reinforced with light tubes and plates for distributing the load at the points of stress concentration.

IV. SUMMARY

To date, the study program has covered the preliminary analysis of the various components included in the VOIS, and a tentative set of specifications has resulted from this analysis. Table IV-1 lists these specifications. For the next period of the study, a more detailed analysis of these components will be conducted so that final specifications for the VOIS may be derived. The areas to be covered during the next period are as follows:

1. Systems Analysis:

   a. Ground data handling and the requirement for picture rectification and identification.

   b. Programming and control functions in the VOIS.

   c. The effect of perturbations on the orbit.

   d. Error analysis of the image-motion compensation.

   e. The resolution capabilities of the over-all system in terms of image recognition. This includes the effects of the various apertures in the system and their contributions to the over-all signal-to-noise ratio.

   f. The required pointing resolution level for selection of areas for high-resolution readout. With regard to this, the use of the RCA TV simulator will be required.

2. Transmission System:

   a. The effect of the electrostatic-tape response as a function of spatial frequency and its effect on the transmission system.

   b. Pre-emphasis as a means to improve picture quality.

   c. Special transmitter and modulator design problems associated with the VOIS encoding systems.

   d. Continued parametric design of the communications system as more detailed data on the DSIF becomes available.

3. Electrostatic Tape Camera:

   a. Electron-gun designs and the simplest means of obtaining the various resolution levels required.

b. Optimum scanning rates to conform to the high-resolution readout requirement.

c. Specifications for the basic circuitry, which will include video amplifiers, focus supplies, deflection generators, and sync and blanking generators.

d. Methods for tape-frame positioning and the requirement for programming.

e. General design techniques for tape transport and take-up reels, including the maximum amount of tape capacity possible.

f. Environmental specifications for the tape camera, including the techniques for sterilization which might be used.

4. Optics:

a. The area of maintaining optical-axis alignment and the control requirements for each of the components of the optical system will be given special attention. In this respect, the effect of thermal variations and vibration will be analyzed.

b. Techniques for obtaining stereoscopic viewing with respect to contour mapping, and qualitative stereoscopic viewing will be delineated along with an analysis of the stereoscopic resolution.

c. The lens aberration coefficients and their effect on off-axis imaging.

d. The physical optical parameters and the requirements for varying the image illumination.

Table IV-1

Preliminary VOIS Characteristics

Average Orbital Altitude (km)	200
Orbital Period (seconds)	7657
Percent Transmission Time	60
Sensor	70-mm electrostatic Tape (60-mm active surface)
Limiting Resolution	200 TV lines/mm
Sensitivity (ft-candle-sec)	0.002
Wavelength Response (microns)	0.5 to 0.7
Tape Capacity	3000 feet
Method of Exposure	Slit and moving Tape
Optics	Baker catadioptric
Focal Length (mm)	914.4
Focal Ratio	F/2.5
Exposure Time (sec)	4×10^{-3}
Video Bandwidth (kilocycles)	500
Resolution per TV line	
High Resolution (meters)	1
Mapping Resolution (meters)	~10
Pointing Resolution (meters)	~100
Camera Weight (pounds)	80
Optics Weight (pounds)	125
Control Circuitry (pounds)	10
Structure (pounds)	~100

Table IV-1 Continued

Average Power (watts)	
Camera	50
Transmitter	150
Control Circuitry	10
Volume (cubic feet)	
Camera	8 (4' x 2' x 1')
Optics	~12 (cylinder 2' diameter by 4' length)
Temperature Control	0 to 50° centigrade
Radiation	Insensitive to the equivalent of Van Allen radiation.